

# Efficient Gluing of Numerical Continuation and a Multiple Solution Method for Elliptic PDEs

Christian Kuehn\*

October 21, 2014

## Abstract

Numerical continuation calculations for ordinary differential equations (ODEs) are, by now, an established tool for bifurcation analysis in dynamical systems theory as well as across almost all natural and engineering sciences. Although several excellent standard software packages are available for ODEs, there are - for good reasons - no standard numerical continuation toolboxes available for partial differential equations (PDEs), which cover a broad range of different classes of PDEs automatically. A natural approach to this problem is to look for efficient gluing computation approaches, with independent components developed by researchers in numerical analysis, dynamical systems, scientific computing and mathematical modelling. In this paper, we shall study several elliptic PDEs (Lane-Emden-Fowler, Lane-Emden-Fowler with microscopic force, Caginalp) via the numerical continuation software `pde2path` and develop a gluing component to determine a set of starting solutions for the continuation by exploiting the variational structures of the PDEs. In particular, we solve the initialization problem of numerical continuation for PDEs via a minimax algorithm to find multiple unstable solution. Furthermore, for the Caginalp system, we illustrate the efficient gluing link of `pde2path` to the underlying mesh generation and the FEM MatLab `pdetoolbox`. Even though the approach works efficiently due to the high-level programming language and without developing any new algorithms, we still obtain interesting bifurcation diagrams and directly applicable conclusions about the three elliptic PDEs we study, in particular with respect to symmetry-breaking. In particular, we show for a modified Lane-Emden-Fowler equation with an asymmetric microscopic force, how a fully connected bifurcation diagram splits up into C-shaped isolas on which localized pattern deformation appears towards two different regimes. We conclude with a section on future software development issues that would be helpful to be addressed to simplify interfaces to allow for more efficient, time-saving, gluing computation for dynamical systems analysis of PDEs in the near future.

**Keywords:** Elliptic PDE, numerical continuation, `pde2path`, minimax, gluing computation, Lane-Emden-Fowler, Caginalp, patterns, bifurcation, FEM, symmetry-breaking.

---

\*Institute for Analysis and Scientific Computing, Vienna University of Technology, 1040 Vienna, Austria

# 1 Introduction

One of the most common problems encountered in the analysis of differential equations arising in applications is to give a qualitative description of the influence of parameters  $\mu \in \mathbb{R}^p$  on the system dynamics. For ordinary differential equations (ODEs) with phase space variables  $x \in \mathbb{R}^N$ , one approach to this problem is to use a standard numerical integration method in combination with Monte-Carlo simulation. For obtaining a basic idea about the system dynamics and exploration of different regimes, this approach is an indispensable tool in modern scientific computing. However, to completely map out the different dynamical regimes in parameter space, this approach requires a systematic simulation over grids of initial values as well as over grids in parameter space. Even though there are techniques available to alleviate some of the computational effort when  $p$  and  $N$  are large (formally we write this as  $p, N \gg 1$ ), such as multi-level Monte Carlo (MC) [55] and quasi-MC [21], the computational effort can still be substantial. In addition, manual inspection of trajectories is usually required to detect important invariant sets, metastable states, bifurcations or locally invariant manifolds, which characterize the dynamics. Therefore, direct simulation can be a computation- and labor-intensive approach to determine dynamical structures in nonlinear systems<sup>1</sup>. Indeed, this problem is well-known for some time as discussed in [101, p.1-2]: *“However, these [time-stepping] techniques rely on waiting out slow exponential decay, or on arduous binary searches, and make highly inefficient use of both machine and human resources.”*

As an alternative, numerical continuation methods are frequently used across all the natural sciences and engineering to systematically explore parameter space for important dynamical structures [70, 73, 90, 96]. This approach has been pioneered in the late 1970s, particularly by Keller [62, 63, 65]. The main idea is to use a predictor-corrector scheme in combination with singularity detection to track parametrized curves (or higher-dimensional manifolds) of solutions to nonlinear algebraic systems arising, e.g., from the steady state formulation of the differential equation. The theory of numerical continuation is well-established by now [2, 39, 40, 49]. For ODEs, it has been used to compute, e.g., bifurcation diagrams [41, 74], stable/unstable manifolds [68, 69], global homoclinic/heteroclinic orbits [18, 24], canards and canard values in fast-slow systems [35, 71], invariant tori [93], spectra [88] and higher-dimensional solution manifolds [56]. There are also several highly successful software packages available for ODE continuation problems such as `AUTO` [42], `XPP` [45], `MatCont` [36] or `PyDSTool` [31]. A key reason, why one may provide excellent self-contained tools for ODEs, as evidenced by the structure of `AUTO` [42], is that many questions may be formulated in terms of classical two-point boundary value problems (BVPs) [7]. Although providing a suitable problem reformulation is not a trivial task, there is substantial practical evidence that the strategy to continue two-point boundary-value problems is very successful<sup>2</sup>.

Furthermore, similar approaches as for ODEs have also been implemented for delay differential equations (DDEs) [44, 97] and have shown promise to also work for stochastic

---

<sup>1</sup> The MC approach with manual inspection of orbits is actually used very successfully - particularly in many application areas - via a method that could be called gsMC (graduate student Monte-Carlo).

<sup>2</sup>One may borrow terminology from physics and describe the situation regarding two-point BVPs as the main “universality class” in dynamical systems computation for ODEs.

differential equations (SDEs) [14, 72]. Hence, it is quite natural to also consider partial differential equations and numerical continuation. This approach has been carried out, e.g., for the Ginzburg-Landau equation [94], excitable media [13, 66], thin film equations [17], the Swift-Hohenberg equation [10, 80], two-dimensional ocean models [61], the Schnakenberg system [102], among certainly many other systems. However, there is no uniform approach via a single software package and/or continuation toolbox available.

In fact, it is unlikely that we are ever going to reach a similar status in terms of stand-alone software, as e.g. `AUTO` and `MatCont` for ODEs, in the case of numerical continuation for PDEs, not even for the stationary case. The main reason is that for each class of PDEs, each type of spatial domain and each type of boundary conditions, there is an vast number of different spatial discretization methods available such as finite element methods (FEM) [20], finite-volume methods (FVM) [75], finite-difference methods (FDM) [99], spectral methods [48], and many others [5, 11, 32, 87]. Furthermore, problems arise on the linear algebra side, when trying to solve large linear systems arising from various discretizations [19, 37]. Given a PDE from applications, the natural question is, what method to use within a numerical continuation framework? The answer clearly is: It depends! Indeed, the various classes of PDEs are so different from a numerical analysis viewpoint, that all we may hope for is to have several software libraries available, one for each class and each method. If we want to combine numerical continuation with numerical PDE techniques, there are two natural approaches. One may just implement the discretization scheme for the PDE “by-hand” for each problem and then add on top of this scheme “by-hand” a numerical continuation approach. This has been used successfully in the PDE continuation examples mentioned above. However, the potential drawback is cost: namely computational cost due to potentially sub-optimal implementation of each component and labor cost due to the programming from first principles. The last issue was nicely formulated - in a slightly different context - by Bangerth and Heister [12]; just one important quote from their opinion piece summarizes the situation well: *“If every graduate student writes the code for a new discretization from scratch, we will be stuck forever solving ‘toy problems’ (like the proverbial ‘Laplace equation on the square’). Unfortunately, this is no longer sufficient to convince our colleagues in the applied sciences [...] that the new method is also applicable to their vastly more complex problems.”*<sup>3</sup>

It is one main aspect - among several - of this paper to show that the combination of numerical continuation, PDE discretization, scientific software packages and suitable gluing codes, is a convincing strategy to solve relatively complex problems at low computational and low labor costs. Of course, one may argue that *in mathematical theory* there is no problem with this well-known idea, it does work. However, *in numerical practice*, the situation is quite different. Even though software for gluing computations within a certain framework, such as `Trilinos` [57], are available, there are still major practical problems to be solved for dynamical systems analysis of PDEs. However, to illustrate that we are right now in the situation, where aiming to glue several algorithms and software packages in an efficient way, can be successful, we study here various elliptic PDEs: the Lane-Emden-Fowler equation [25, 106] with a linear term, the Lane-Emden-Fowler equation with a localized force and the Caginalp system [22, 23]. The main computational framework is set up in `MatLab` as

---

<sup>3</sup>One may view the described situation as another incarnation of gsMC.

a high-level gluing language with a focus on the recently developed numerical continuation software `pde2path` [103, 43].

It is well-known by users of numerical continuation software that, during the practical implementation process, finding starting solutions is a key obstacle as pointed out nicely by Sandstede and Lloyd [92]: “*Strategies for finding good initial guesses depend strongly on the underlying specific problem: often, finding good starting data is the main obstacle for using [numerical continuation] successfully*”<sup>4</sup>. Here we address this problem by using a minimax approach to variational elliptic PDE proposed by Zhou and co-workers [76, 77] by employing the code [108] to generate starting solutions in `pde2path`, i.e., instead of programming the continuation method “by-hand” [27] we glue the available combination of FEM, continuation and variational optimization to minimize the programming effort. The goal is to demonstrate that already today many computational tasks could be simplified substantially if better interfaces for gluing code would be available, and new code would be designed with this problem in mind.

To cross-validate the gluing approach, we use the Lane-Emden-Fowler equation, which is a standard example exhibiting multiple (unstable) solutions, which are computable by the `minimax` method [76, 108]. We add a linear term term, whose rate is used as the main continuation parameter. Starting solutions are first determined by the `minimax` approach and then continued in `pde2path`. As a second approach, the homogeneous zero solution branch is continued numerically, and branch switching is performed at bifurcation points to calculate branches, which each contain a single solution to the Lane-Emden-Fowler equation without the added linear term.

As the first main new problem for this paper, we consider the Lane-Emden-Fowler equation with a forcing term. The motivation for modifying the elliptic PDE with a certain forcing term is developed by pointing out the analogy to a similar term appearing as a localized microforce in the generalized Ginzburg-Landau/Allen-Cahn equation [1, 4, 52, 54], where the nonlinearity has the opposite sign of the Lane-Emden-Fowler equation. Although the theory of the two classes is quite different due to the different signs of operators [26], the algebraic structure is similar and the motivation of external microforces also applies to fluid dynamics applications of the Lane-Emden-Fowler equation. As before, we use a `minimax` approach to determine a set of starting solutions. In this case, there is no homogeneous solution branch available for direct numerical continuation, although a two-parameter homotopy approach could be tried to locate starting solutions<sup>5</sup>. We show that there is a quite intricate deformation of localized structures along isolated bifurcation curves. The bifurcation curves are C-shaped curves, which deform onto thinner structures in the  $L^\infty$ -norm as the complexity of the patterns is increased. In particular, the numerical study in this paper illustrates the effect, how symmetry-breaking may occur when asymmetric localized forces are added to elliptic PDEs on symmetric domains. From an analytical viewpoint, special solutions of nonlinear elliptic PDEs on symmetric domains are a very active research area, see e.g. [15]. The same remark applies to the singularly-perturbed elliptic PDE related to

---

<sup>4</sup> The original quote contains [AUTO] instead of [numerical continuation] but it is clear that the problem will persist from a particular software package to the more general problem of determining starting solutions.

<sup>5</sup>This approach becomes from a practical implementation viewpoint more involved, which is exactly what we aim to avoid here.

Lin-Ni-Takagi type problems [3, 78, 79], which has the same signs for the operators as our modified Lane-Emden-Fowler equation without the asymmetric microforce. Hence, it is critical to understand, for applications and theory, the effect how inhomogeneous bifurcation branches continue globally under microforce loading.

As a third case study, we consider the Caginalp system for phase transitions, such as melting-solidification processes. The domain is chosen as a more complex, wing-shaped geometry. The motivation for this setup arises directly from (de-)icing problems in aerospace engineering. As for the previous elliptic PDEs, there are multiple solutions for a fixed parameter value, which we compute using `pde2path` by guessing the right starting solution. The `minimax` approach using the code [108] does not modify in a straightforward way to detect the solutions. Therefore, a more elaborate programming effort would be required to use the variational starting point, which is precisely what we want to avoid here. However, from various recent works, e.g. [107], one does expect that it is possible to modify the approach to the Caginalp system, as well as other variational problems to find starting solutions for continuation; this approach will be considered in future work. For the Caginalp system we find an interesting bifurcation diagram with potential applications to tune parameter values to access different parts of the so-called mushy regime between melting and solidification.

In the last part of the paper, we provide a very brief overview of various software developing issues for gluing codes in numerical continuation analysis of PDEs. The idea is to just record, which aspects have been important to facilitate the simplest possible combination of various algorithms used in this work. The second goal is to provide a more detailed outlook, from the viewpoint of gluing computation and an end-user perspective of applied nonlinear dynamics, to help developers improve future software releases. It is hoped that this may help to facilitate the exchange of differential equations software between different research communities.

The paper is structured as follows: In Section 2 we review the basic numerical tools very briefly and fix the notation. The cross-validation test problem is considered in Section 3. The bifurcation analysis for the Lane-Emden-Fowler equation with a linear term and a localized microforce asymmetric load is carried out in Section 4. Numerical accuracy and performance results for the algorithms used in this example, are recorded in Appendix A. The Caginalp system on an airplane-shaped geometry is numerically studied in Section 5. Section 6 contains a summary of the main software issues encountered while carrying out the computations. We conclude with a short summary in Section 7.

## 2 Basic Review of Methods

In this section, we shall just provide a very quick review of the computational tools we are going to use in the gluing-type numerical continuation calculations for elliptic PDEs. Consider a bounded domain  $\Omega \subset \mathbb{R}^2$ ,  $x = (x_1, x_2)^\top \in \Omega$  and  $u = u(x) \in \mathbb{R}$ . We shall assume that the boundary  $\partial\Omega$  is piecewise smooth throughout this paper. In this paper, we shall

restrict<sup>6</sup> to elliptic PDEs [46, 47] of the form

$$-c\Delta u(x) + au(x) - f(u(x), x, \mu) = 0, \quad x \in \Omega \subset \mathbb{R}^2 \quad (1)$$

where  $a \in \mathbb{R}$ ,  $c \in (\mathbb{R} - \{0\})$ ,  $f : \mathbb{R}^3 \rightarrow \mathbb{R}$  is sufficiently smooth,  $\mu \in \mathbb{R}$  is the main bifurcation parameter, and  $\Delta = \frac{\partial^2}{\partial x_1^2} + \frac{\partial^2}{\partial x_2^2}$  is the usual Laplacian. Furthermore, (1) will be augmented with either zero Dirichlet or Neumann boundary conditions, i.e., we consider

$$u(x) = 0 \quad \text{for } x \in \partial\Omega \quad \text{or} \quad (\vec{n} \cdot \nabla u)(x) = 0 \quad \text{for } x \in \partial\Omega, \quad (2)$$

where  $\vec{n} \in \mathbb{R}^2$  denotes the outer unit normal vector to  $\Omega$ ,  $\nabla u = \left( \frac{\partial u}{\partial x_1}, \frac{\partial u}{\partial x_2} \right)^\top \in \mathbb{R}^2$  is the gradient of  $u$ , and ‘ $\cdot$ ’ denotes the standard Euclidean inner product.

## 2.1 FEM for Elliptic PDE & pdetoolbox

The main underlying PDE solver used for (1), via the numerical continuation software `pde2path`, is the MatLab `pdetoolbox` [81, 82]. A standard finite-element method (FEM) is used in the `pdetoolbox`, which we very briefly recap here to fix some notation in the case of Dirichlet boundary conditions. Let  $H_0^1 = H_0^1(\Omega)$  denote the usual Sobolev space

$$H_0^1 = \{v \in L^2(\Omega) : \nabla v \in L^2(\Omega), v|_{\partial\Omega} = 0\}. \quad (3)$$

Let  $\mathcal{T} = \{T_i\}_{i=1}^{n_t}$  be a triangulation of  $\Omega$  consisting of  $n_t$  triangles  $T_i$  and let  $\mathcal{N} = \{p_k\}_{k=1}^{n_p}$  denote the set of  $n_p$  associated node/vertex points  $p_k \in \mathbb{R}^2$ . Of course,  $n_p$  can potentially be very large if a fine mesh is needed to correctly resolve solutions. Then define the space of piecewise-linear finite elements

$$V_h := \{v \in C(\Omega) : v|_{T_i} \text{ is affine linear for all } T_i \in \mathcal{T}\}, \quad (4)$$

where the subscript  $h$  usually indicates the size of the triangles, e.g.,  $h$  can be taken as the maximum edge length.

The weak formulation of (1), with a test function  $v_h \in V_h$ , is

$$\int_{\Omega} [c(\nabla u \cdot \nabla v_h)(x) + au(x)v_h(x)] dx = \int_{\Omega} v_h(x)f(u(x), x, \mu) dx, \quad \forall v_h \in V_h. \quad (5)$$

We want to approximate the true solution  $u$  by its representation  $u_h$  in  $V_h$  given by

$$u_h(x) = \sum_{k=1}^{n_p} U_k \phi_k(x) \quad (6)$$

using the nodal basis functions  $\phi_k \in V_h$ , which are defined via the condition  $\phi_k(p_j) = \delta_{k,j}$ , where  $\delta_{k,j}$  is the usual Kronecker delta with  $\delta_{k,k} = 1$  and  $\delta_{k,j} = 0$  if  $k \neq j$ . Inserting  $u_h \approx u$  into (5) and using  $v_h = \phi_k$  as test functions for each  $k$ , leads to a nonlinear system

$$KU = F(U, \mu) \quad \text{or} \quad KU - F(U, \mu) = 0, \quad (7)$$

---

<sup>6</sup>The idea, and most of the software components, would also work for systems of elliptic PDEs. However, it is the goal of this paper to show, how simple gluing computation can be, not how difficult it can be made.

where  $U = \{U_k\}_{k=1}^{n_p} \in \mathbb{R}^{n_p}$  is the vector of unknowns and  $K \in \mathbb{R}^{n_p \times n_p}$ ,  $F : \mathbb{R}^{n_p} \times \mathbb{R} \rightarrow \mathbb{R}^{n_p}$  are assembled automatically in the `pde toolbox`, i.e., this is the key step, which can be very different for various methods as well as different types of PDEs.

In addition to mesh generation and assembly of the linear system, the `pde toolbox` also provides an adaptive mesh refinement algorithm [59] based on the error estimator

$$E_i = E(T_i) = \alpha \|h(f - au_h)\|_{L^2(T_i)} + \beta c \left( \frac{1}{2} \sum_{\tau \in \partial T_i} h_\tau^2 [\vec{n}_\tau \cdot \nabla u_h]^2 \right)^{1/2}, \quad (8)$$

where  $\vec{n}_\tau$  is the outer unit normal and  $h_\tau$  the length of the edge  $\tau$ ,  $h = h(x)$  is the local mesh size for the element  $T_i$ , the term  $[\vec{n}_\tau \cdot \nabla u_h]$  denotes the flux across the element edge, and  $\alpha, \beta$  are fixed constants. In practice, one of the most efficient schemes is to equidistribute the error and split those triangles, and relevant adjacent ones, with the highest errors during a mesh refinement step. The error equidistribution principle has been used for a long time in numerical continuation problems for BVPs of ODEs motivated by the COLSYS code [6], which pre-dates the development of AUTO [42]. Of course, we are again faced with a similar challenge as in the discretization step for PDEs as there is a huge variety of ideas and estimators for mesh adaptation, not just the solution (8) implemented in the `pde toolbox`.

## 2.2 Numerical Continuation & pde2path

Here we briefly review the numerical continuation algorithm used in `pde2path` [103]; for more theoretical background see [49, 74]. For numerical continuation, one views the problem (1) as a mapping

$$g(u, \mu) := -c\Delta u(x) + au(x) - f(u(x), x, \mu) = 0, \quad g : \mathcal{H} \times \mathbb{R} \rightarrow \mathcal{H}, \quad (9)$$

where we assume, for simplicity, that  $\mathcal{H}$  is a Hilbert space, e.g.,  $\mathcal{H} = H_0^1(\Omega)$ . The goal is to trace out a curve (or branch)  $z(s) := (u(s), \mu(s)) \in \mathcal{H} \times \mathbb{R}$  of solutions to  $g(u, \mu) = 0$ , where  $s$  is arclength. However, working in the abstract setting does not lead immediately to an implementable numerical algorithm and one has to consider the problem via a spatial discretization as in (7) so one studies

$$G(U, \mu) := KU - F(U) = 0, \quad G : \mathbb{R}^{n_p} \times \mathbb{R} \rightarrow \mathbb{R}^{n_p}, \quad (10)$$

where the Hilbert space is just a, potentially very large, Euclidean space  $\mathbb{R}^{n_p}$ . The goal is still to trace out a curve  $Z(s) := (U(s), \mu(s)) \in \mathbb{R}^{n_p} \times \mathbb{R}$ . To make  $s$  an approximation to arclength, one augments (10) by an extra condition and studies

$$H(U, \mu) := (G(U, \mu), p(U, \mu, s))^\top = 0, \quad (11)$$

where  $p : \mathbb{R}^{n_p} \times \mathbb{R} \times \mathbb{R} \rightarrow \mathbb{R}$  will be defined below. Suppose we know a point  $(U(s_0), \mu(s_0)) =: (U_0, \mu_0)$  on the curve  $Z = Z(s)$  at  $s = s_0$  from some initial guess or otherwise<sup>7</sup>. Note that

---

<sup>7</sup>Recall from Section 1 that this is already a crucial assumption; we are going to find initial solutions in Section 2.3 using a specialized algorithm.

we may compute the tangent vector

$$\dot{Z}_0 := (\dot{U}_0, \dot{\mu}_0)^\top := \left( \left. \frac{d}{ds} U(s) \right|_{s=s_0}, \left. \frac{d}{ds} \mu(s) \right|_{s=s_0} \right)^\top \in \mathbb{R}^{n_p+1} \quad (12)$$

to  $Z(s)$  at  $s = s_0$  by differentiating  $G(U(s), \mu(s)) = 0$  with respect to  $s$  at  $s_0$  so that

$$(DG)|_{s=s_0} \dot{Z}_0 = 0, \quad (13)$$

where  $(DG)|_{s=s_0}$  is the total derivative of  $G$  at  $s_0$ , i.e., finding  $\dot{Z}_0$  reduces to solving the linear system (13). Then, define

$$p(U, \mu, s) := \xi \dot{U}_0 \cdot (U(s) - U_0) + (1 - \xi) \dot{\mu}_0 (\mu(s) - \mu_0) - (s - s_0), \quad (14)$$

where  $\xi$  is an algorithm parameter with  $0 < \xi < 1$ . In `pde2path`,  $\xi$  is a key parameter to “tune” or “control” the behavior of the numerical continuation algorithm and it is assumed that  $\dot{Z}_0$  is normalized to one in the weighted  $\xi$ -norm derived from the inner product

$$\langle (U, \mu)^\top, (W, \nu)^\top \rangle_\xi := \xi U \cdot W + (1 - \xi) \mu \nu, \quad \|\dot{Z}_0\| = \sqrt{\langle \dot{Z}_0, \dot{Z}_0 \rangle_\xi} \stackrel{!}{=} 1. \quad (15)$$

Then  $p(U, \mu, s) = 0$  defines a hyperplane perpendicular, with respect to the inner product  $\langle \cdot, \cdot \rangle_\xi$ , to  $\dot{Z}_0$  at a distance  $\delta s := s - s_0$  from  $(U_0, \mu_0)$ . Now, one can finally define the main predictor-corrector steps to compute a new point

$$(U_1, \mu_1)^\top := (U(s_1), \mu(s_1))^\top = (U(s_0 + \delta s), \mu(s_0 + \delta s))^\top. \quad (16)$$

The prediction step is to set  $(U^1, \mu^1)^\top := (U_0, \mu_0)^\top + \delta s \dot{Z}_0$ . One possibility to carry out the correction step is to use a straightforward Newton iteration

$$\begin{pmatrix} U^{j+1} \\ \mu^{j+1} \end{pmatrix} = \begin{pmatrix} U^j \\ \mu^j \end{pmatrix} - \left( \begin{array}{cc} D_u G & D_\mu G \\ \xi \dot{U}_0 & (1 - \xi) \dot{\mu}_0 \end{array} \right) \Big|_{(U^j, \mu^j)} H(U^j, \mu^j) \quad (17)$$

Terminating Newton’s method at some step  $j = J_1$  by a suitable error criterion, we set  $(U_1, \mu_1) := (U^{J_1}, \mu^{J_1})$ . So the key algorithm control parameters for the `pde2path` implementation of numerical continuation are the step size  $\delta s$ , the criterion for terminating Newton’s method and the parameter  $\xi$ , which basically balances vertical versus horizontal preference along bifurcation curves [103].

Of course, there are many different variations one may use, e.g., approximating the Jacobian in Newton’s method in different ways [37], use Moore-Penrose continuation [74] or replace the Newton method by, a sometimes more robust, secant approach. Another issue are bifurcation points [74], where one also wants an algorithm to switch between different bifurcation branches; we refer the reader for details of these algorithms to [74, 49] as this is not the main problem considered in this paper.

## 2.3 Multiple Starting Solutions & minimax

As discussed in Section 1 and mentioned in Section 2.2, one main challenge in numerical continuation is to find at least one starting solution. Even if one solution can be guessed, or an algorithm does converge to a solution from a rough initial guess, this is often not sufficient. Indeed, frequently not all bifurcation branches connect to a single branch on which the single known solution lies, or it is very difficult to trace out all solutions from a single branch using standard branch switching approaches [42]. For example, isolated bifurcation branches, so-called isolas [9, 64], appear frequently in applications [16, 34, 67, 83]. In fact, in two-dimensional spatial problems one may potentially find isola structures more easily [98], in comparison to the one-dimensional case<sup>8</sup>.

One approach to systematically look for starting solutions for elliptic PDEs of the form (1) is to consider the associated energy variational functional. For zero Dirichlet boundary conditions, consider the space  $\mathcal{H} = H_0^1$  and the functional

$$J(u) := \int_{\Omega} \left[ \frac{c}{2} \nabla u(x) \cdot \nabla u(x) + \frac{a}{2} (u(x))^2 - F(u(x), x, \mu) \right] dx, \quad (18)$$

where  $F$  is the anti-derivative of  $f$  with respect to the  $u$ -component, i.e.,

$$F(u(x), x, \mu) := \int_0^{u(x)} f(w, x, \mu) dw. \quad (19)$$

When dealing with the energy functional  $J(u)$ , we shall always assume that the bifurcation parameter  $\mu$ , as well as the other parameters  $a, c$ , are fixed so we suppress the dependence in the notation; in particular, we are going to search for a set of starting solutions for fixed parameter values.

Let  $J'(u) \in \mathcal{H}$  denote the Fréchet derivative of  $J$  at  $u$ . Solutions  $u$  of the Euler-Lagrange equation  $J'(u) = 0$  are also called critical points. Recall that

$$\int_{\Omega} J'(u)v dx = \lim_{\epsilon \rightarrow 0} \frac{J(u + \epsilon v) - J(u)}{\epsilon} = \int_{\Omega} g(u, \mu)v dx \quad (20)$$

where  $g(u, \mu) = 0$  is the original elliptic PDE, i.e., critical points are weak solutions and vice versa [46]. By elliptic regularity [46], weak solutions are smooth classical solutions. In general, critical points can be maxima, minima or saddle points. A critical point is non-degenerate if the second Fréchet derivative  $J''(u)$  exists and is invertible. The Morse index (MI) of a non-degenerate critical point is defined as the maximal dimension of a subspace on which  $J''(u)$  is negative definite<sup>9</sup>. If  $\text{MI} = 0$ , then we have a stable minimum for the gradient flow of the energy. For  $\text{MI} > 0$  there is at least one unstable direction.

Note that minima are relatively easy to find by steepest descent but that saddle points are more challenging, particularly if one wants to find multiple ones for fixed parameters.

---

<sup>8</sup>Quoting from [98] in the context of a Swift-Hohenberg equation: “*Isolas appear for some non-periodic boundary conditions in one spatial dimension but seem to appear generically in two dimensions.*”

<sup>9</sup>Of course, this situation can nicely be imagined geometrically for the finite-dimensional case [60].

Li and Zhou [76, 77], motivated by the work in [29, 38], developed an algorithm to compute multiple saddle solutions. We shall only outline the basic proposed strategy here; for details see [76, 77]. Let  $\tilde{\mathcal{H}} \subset \mathcal{H}$  be a subspace of the Hilbert space  $\mathcal{H}$  and consider the unit sphere  $S_{\tilde{\mathcal{H}}} := \{v \in \tilde{\mathcal{H}} : \|v\|_{\mathcal{H}} = 1\}$ . Let  $\mathcal{L}$  be a closed subspace in  $\mathcal{H}$  with orthogonal complement  $\mathcal{L}^\perp$ . For each  $v \in S_{\mathcal{L}^\perp}$ , define the closed half-space

$$[\mathcal{L}, v] := \{tv + w : w \in \mathcal{L}, t \geq 0\}. \quad (21)$$

A set-valued map  $P : S_{\mathcal{L}^\perp} \rightarrow 2^{\mathcal{H}}$  is called the peak mapping of  $J$  with respect to  $\mathcal{L}$  if for any  $v \in S_{\mathcal{L}^\perp}$ ,  $P(v)$  is the set of all local maximum points of  $J$  in  $[\mathcal{L}, v]$ . Essentially, the map  $P$  collects local maxima in a half-space. A single-valued map  $p : S_{\mathcal{L}^\perp} \rightarrow \mathcal{H}$  is a peak selection of  $J$  with respect to  $\mathcal{L}$  if

$$p(v) \in P(v), \quad \forall v \in S_{\mathcal{L}^\perp}. \quad (22)$$

Basically  $p$  selects a single maximum parametrized by  $v$ ; the notion of peak selection can be localized by intersecting the relevant sets with neighbourhood of  $v$  [76, 77]. The main idea of finding critical points is to restrict to suitable solution submanifolds

$$\mathcal{M} := \{p(v) : v \in S_{\mathcal{L}^\perp}\}. \quad (23)$$

Essentially, one would like to think of the manifold  $\mathcal{M}$  as (an approximation to) the stable manifold of a saddle critical point. Then one may use a descent method on  $\mathcal{M}$ , in combination with a method to stay on  $\mathcal{M}$  during the iteration, to find the saddle point. Of course, one has also to avoid convergence to a saddle point, which has been found previously. The descent process is a minimization problem and the step to return to  $\mathcal{M}$  is carried out via a maximization problem, leading to a `minimax`-type algorithm. The span of the previously found solutions is the space  $\mathcal{L}$ , which one tries to avoid at future iteration steps, i.e., the search essentially works in the complementary half-space  $[\mathcal{L}, v]$ .

Note that the algorithm just outlined, can be viewed as a descent method with a constraint to stay inside a certain search space by excluding previously found directions. The entire procedure is easily implemented via FEM as the FEM discretization just reduces the original problem to a discrete finite set of values of  $u$  at certain points. Then one has to actually solve a large, but finite-dimensional, constrained optimization problem. A detailed algorithmic description can be found in [76, 77], the implementation of the `minimax` algorithm we use here is [108], while a number of applications of the method are discussed, e.g., in [27, 28, 105, 107].

It is desirable to try to glue the variational `minimax` approach to a standard continuation package, which itself is glued to a standard FEM package. This is precisely, what is carried out in practice here for several problems using `pde2path` as the main focal point. For more details on the scientific computing challenges involved, we refer to Section 6.

### 3 A Cross-Validation Test Problem

As a first step, we are going to compare, for a test problem from the class of elliptic PDEs (1), two different approaches:

- (I) Use the `minimax` approach to calculate at a fixed parameter value  $\mu_0 = \mu(s_0)$  several starting solutions  $u_0^l = u_0^l(x)$ ,  $l \in \{1, 2, \dots, L\}$  for some  $L \geq 2$ . Then use numerical continuation for each starting solution, generating multiple solution branches  $Z^l(s) := (u^l(s), \mu^l(s))$ .
- (II) Start with a single, preferably simple and easy-to-guess, solution at a fixed parameter value  $(u_0^*, \mu_0^*)$  and then continue the branch  $Z^*(s) = (u^*(s), \mu^*(s))$ . Via branch switching at bifurcation points, one can then try to recover the starting set of solutions from (I) as points on the branch, i.e.,  $(u^*(s^l), \mu^*(s^l)) = (u_0^l, \mu_0)$  for some values  $s^l$ .

It is helpful to select a test problem, where we may expect that classical continuation ideas using the homotopy approach (II) would suffice, but where the variational problem is nontrivial. As a domain, we choose a rectangle  $\Omega := (-l_{x_1}, l_{x_1}) \times (-l_{x_2}, l_{x_2}) \subset \mathbb{R}^2$ ,  $l_{x_1}, l_{x_2} > 0$ . Consider the elliptic PDE for  $u = u(x)$  given by

$$\begin{cases} 0 = -\Delta u - \mu u - u^3 = g(u, \mu), & x \in \Omega, \\ 0 = u, & x \in \partial\Omega. \end{cases} \quad (24)$$

where  $\mu \in \mathbb{R}$  is the main bifurcation parameter. For  $\mu = 0$ , and multiplying the entire equation by  $-1$ , the PDE (24) is also known as the Lane-Emden-Fowler equation [25, 95, 106]. In fact,  $\mu = 0$  is the standard test case from [108] so we definitely can try to carry out the strategy (I) with  $\mu_0 = 0$ . Furthermore,  $u \equiv 0$  is a solution, so setting  $(u_0^*, \mu_0^*) = (0, 0)$  is a standard starting point for strategy (II).

We start with strategy (I). The variational formulation (18) of (24) via an energy functional is given, for  $u \in H_0^1(\Omega)$  and  $\mu_0 = 0$ , by

$$J(u) = \int_{\Omega} \left[ \frac{1}{2} \|\nabla u(x)\|^2 - \frac{1}{4} u^4(x) \right] dx, \quad (25)$$

where  $\|\cdot\|$  denotes the usual Euclidean norm in  $\mathbb{R}^2$ . The results from the `minimax` algorithm can be reproduced using [108] and are shown in 1(a)-(e) for  $l_{x_1} = 0.5 = l_{x_2}$ . Figure 1(a)-(e) shows four distinct classes of solutions. The solution of Morse index  $MI = 1$  is shown in Figure 1(a). Two solutions with two peaks centered along the coordinate axis of Morse index  $MI = 2$  are shown in Figures 1(c1)-(c2) and the corresponding two-peak solutions with the peaks along the diagonal and anti-diagonal are displayed in Figures 1(b1)-(b2). Then, there are also two different classes of solutions of Morse index  $MI = 4$  shown in Figures 1(d)-(e). Once the starting solutions have been found, they were saved and re-meshed onto a slightly coarser grid for continuation in `pde2path`. Figure 1(f) shows the resulting bifurcation diagram in  $(\mu, \|u\|_{\infty})$ -space, where  $\|\cdot\|_{\infty}$  denotes the usual  $L^{\infty}$ -norm. Figure 1(f) shows the raw output of the `pde2path` continuation, i.e., the actual points computed on the desired seven branches, starting from the seven starting solutions located at  $\mu = 0$ . The  $L^{\infty}$ -norms of the seven starting solutions correspond to lexicographical order of the labels, e.g., the smallest  $L^{\infty}$ -norm is in Figure 1(a), while the largest is in Figure 1(e).

Some of the important algorithmic parameter values for `pde2path` used during the continuation runs were:

$$\xi = 1/n_p, \quad \text{neig} = 100, \quad \text{dsmax} = 0.5, \quad \text{hmax} = 0.1, \quad (26)$$

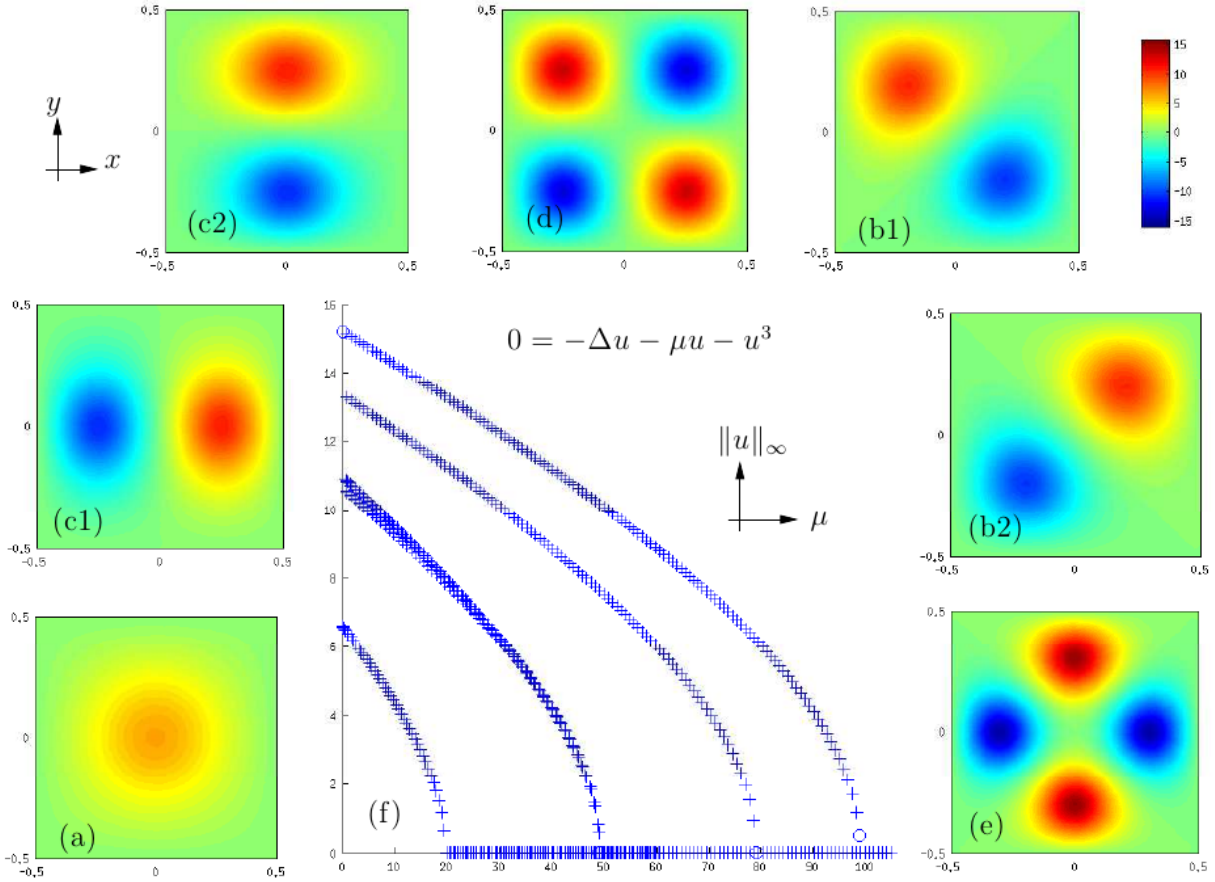


Figure 1: Numerical continuation results for (24) starting from variational solutions found via the `minimax` algorithm at  $\mu = 0$ . The seven starting solutions are shown in (a)-(e). The four double bump solutions (b)-(c) split into two classes with different  $L^\infty$ -norm, where the norm form for (b1)-(b2) is smaller than for (c1)-(c2). The norms for (d) and (e) are the two largest norms. The part (f) of the figure shows the raw output of `pde2path` upon continuation; see also the description in the text.

where `neig` is the number of computed eigenvalues for stability/bifurcation detection, `dsmax` is the maximum step size for  $\delta s$  and `hmax` is the maximum triangle side lengths  $h$  for the (uniform) global triangulation. Otherwise, we used standard parameter values, where it should be noted that using finite-differencing for the Jacobian seemed to yield a more stable algorithm<sup>10</sup>. The results in Figure 1(f) show that all seven initial bifurcation branches connect back to the trivial solution branch at  $(u, \mu) = (0, \mu)$ . We also observed that changing some `pde2path` continuation parameters it was possible to change the direction the zero branch was continued in once it was reached, either to the left or to the right; Figure 1 shows all seven branches going to the right, i.e. increasing  $\mu$ , once the zero branch was reached. There seems to be a numerical artifact for the branch corresponding to the starting

<sup>10</sup>In the forthcoming version `p2p2` of `pde2path` [43], this effect, which arises due to interpolation error, is resolved. I would like to thank Hannes Uecker for explaining me the details behind this observation.

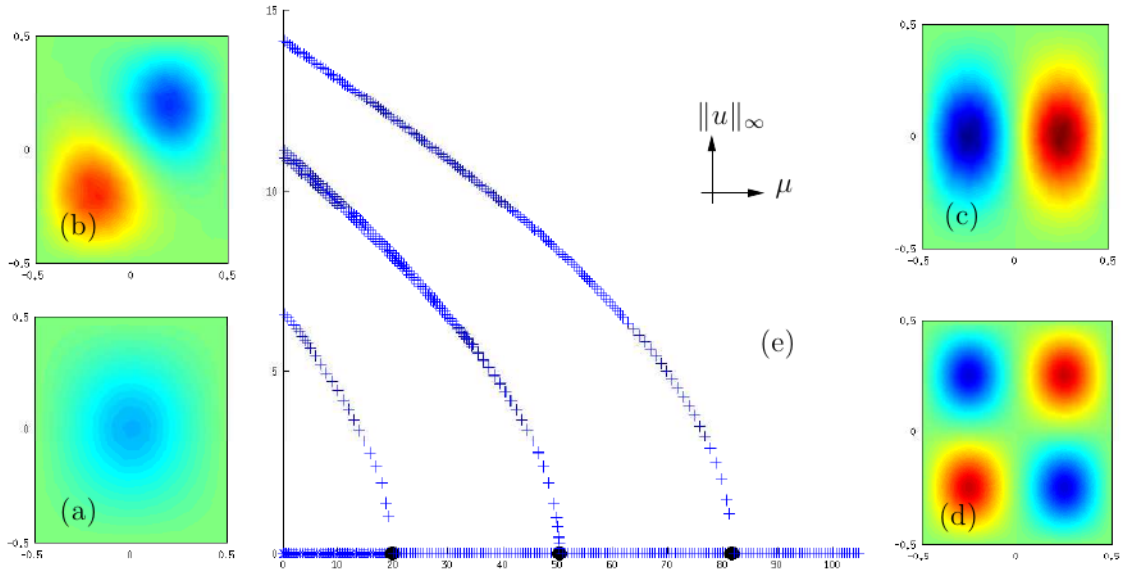


Figure 2: Numerical continuation results for (24) starting from from the zero solution  $u \equiv 0$  at  $\mu = 0$ ; the color coding is as in Figure 1. Further solutions are found by branch switching at four detected bifurcation/branch points (marked as black dots). The four final ( $\mu = 0$ ) solutions on the nontrivial branches are shown in (a)-(d). The two double bump solutions (b)-(c) again have different  $L^\infty$ -norm at  $\mu = 0$ . The branch point for the solution in Figure 1(e) has not been found in a continuation run using the routine `cont`. However, the branch point can be found when using `findbif` and is located at  $\mu \approx 101.218$ . The part (e) of this figure shows the raw output of `pde2path` upon continuation.

solution in Figure 1(e), where a bifurcation point (blue circle) is detected quite a bit before the actual zero branch is reached.

For the second approach (II), we continue the trivial zero branch. The results are shown in Figure 2. Four branch points (black dots) were detected when the continuation was run between  $\mu = 0$  and  $\mu = 110$ ; again, the last bifurcation point corresponding to the diagonal/anti-diagonal  $MI = 4$  solution from Figure 1(e) was not detected using a standard bifurcation run using `cont`. However, this branch point is correctly detected using the routine `findbif`<sup>11</sup>. Branch switching was performed using `pde2path` at the bifurcation points. The new non-trivial solutions were tracked back up to  $\mu = 0$ , which yields the same - up to symmetry - solutions as recorded for approach (I). In summary, both approaches essentially lead to the same results and we have definitely cross-validated (I) and (II).

<sup>11</sup>I would like to thank Hannes Uecker for making me aware of this, i.e., that `findbif` evaluates the eigenvalues, while `cont` checks for a vanishing determinant.

## 4 Adding a Localized Microforce Load

We have observed for the test problem in Section 3 that symmetries lead to difficulties of detection of certain branches as multiple solution branches come together at a single bifurcation point. Hence, it is natural to break the symmetry by a certain perturbation. In [103], the symmetry is broken for a cubic-quintic Ginzburg-Landau/Allen-Cahn type equation of the form

$$\begin{cases} 0 = -c\Delta u - \mu u - u^3 + u^5, & x \in \Omega, \\ 0 = u, & x \in \partial\Omega, \end{cases} \quad (27)$$

on a rectangle  $\Omega := (-l_{x_1}, l_{x_1}) \times (-l_{x_2}, l_{x_2}) \subset \mathbb{R}^2$  with  $l_{x_1} = 1$  and  $l_{x_2} = 0.9$ . Instead of breaking the geometry of the domain, one may also ask, how one expects generic symmetry-breaking for Allen-Cahn/Ginzburg-Landau-type PDEs when the equation itself is perturbed. One possible mechanism can be found in the work of Gurtin [52], who derives the Ginzburg-Landau equation from basic principles of force balance. The basic motivation for Ginzburg-Landau-type models are two-phase systems, whose evolution is described on a macroscopic level by an order parameter  $\rho = \rho(x, t)$  for  $(x, t) \in \Omega \times [0, T]$  for some  $T > 0$ . The force balance equations for a given body lead to the generalized Ginzburg-Landau equation

$$\beta \frac{\partial \rho}{\partial t} = \nabla \cdot \left[ \frac{\partial \Psi}{\partial p}(\rho, \nabla \rho) \right] - \frac{\partial \Psi}{\partial \rho}(\rho, \nabla \rho) + \gamma, \quad (28)$$

where  $p = \nabla \rho$ ,  $\Psi : \mathbb{R}^2 \rightarrow \mathbb{R}$  is a given free energy,  $\gamma$  is an external microforce applied to the body and  $\beta$  is the constitutive modulus as discussed in [52]. Taking a constant positive  $\beta$  and the free energy as  $\Psi(\rho, \nabla \rho) = F(\rho, \mu) + \frac{1}{2}\alpha \|\nabla \rho\|^2$  leads to the Ginzburg-Landau equation with an applied microforce

$$\beta \frac{\partial \rho}{\partial t} = \alpha \Delta \rho - \frac{\partial F}{\partial \rho}(\rho, \mu) + \gamma, \quad (29)$$

where  $\alpha, \beta$  are positive parameters and  $\gamma = \gamma(x)$  is an external microforce on the body. Frequently, the potential  $F$  is chosen as a double-well leading to  $F'(u) = \mu u - u^3$ , which has different signs in comparison to the Lane-Emden-Fowler equation from Section 3. However, the idea that there is a (microscopic) external force acting on the problem still seems very reasonable. Hence, we propose to study the elliptic problem

$$\begin{cases} 0 = -\Delta u - \mu u - u^3 + \gamma, & x \in \Omega, \\ 0 = u, & x \in \partial\Omega, \end{cases} \quad (30)$$

where  $\gamma = \gamma(x)$  depends in a non-trivial way upon the spatial coordinate and  $\Omega := (-l_{x_1}, l_{x_1}) \times (-l_{x_2}, l_{x_2}) \subset \mathbb{R}^2$  with  $l_{x_1} = 1 = l_{x_2}$ . To break the symmetry encountered in Section 3, we propose to consider a point-type load modeled by the function

$$\gamma = \gamma(x) := \begin{cases} \gamma_a \exp(-1/\gamma_b[(x_1 - \gamma_1)^2 + (x_2 - \gamma_2)^2]), & \text{if } x = (x_1, x_2)^\top \in \Omega, \\ 0, & \text{if } x \in \partial\Omega, \end{cases} \quad (31)$$

and we fix  $\gamma_a = 10$ ,  $\gamma_b = \frac{1}{10}$ ,  $\gamma_1 = 0.5 = \gamma_2$ . Note that  $\gamma : \Omega \rightarrow [0, +\infty)$  is basically localized, with respect to numerical accuracy, in a small neighbourhood of the point  $(x_1, x_2) =$

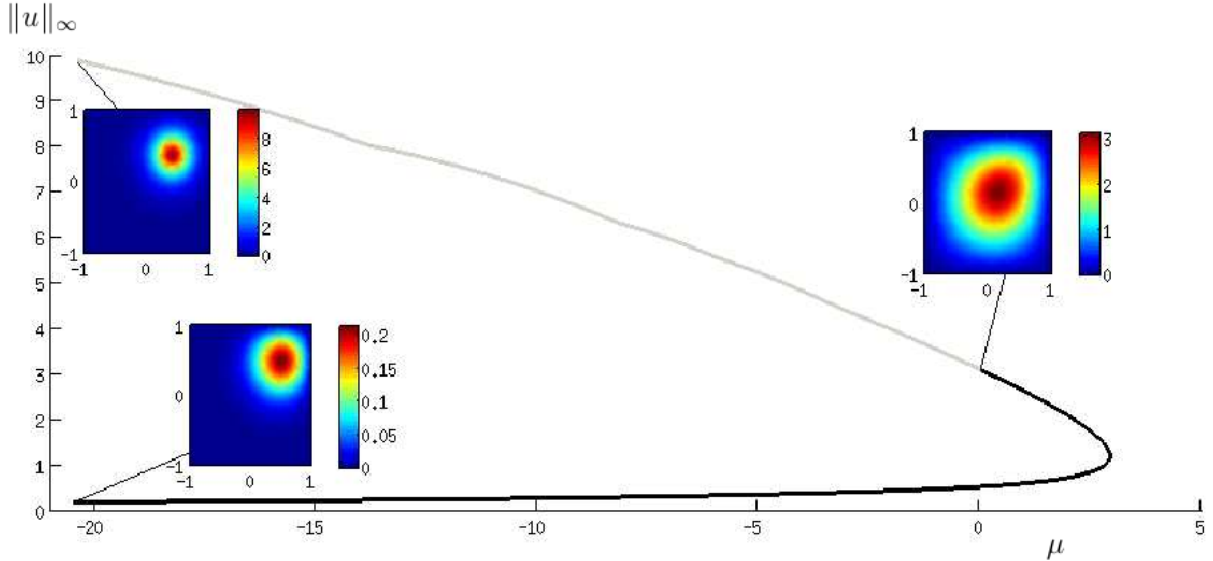


Figure 3: Numerical continuation results for (30) with external force given by (31). The starting solution was obtained by the variational `minimax` approach at  $\mu = 0$ . Then, forward and backward numerical continuation from this starting point leads to two branches (black and grey). The starting solution with Morse index  $MI = 1$  is also shown (on the right side), as well as the two endpoints on the computed branches (on the left side); for a more detailed description see the main text.

(0.5, 0.5). Note carefully that using (31) as the forcing in (30) means that there are no homogeneous constant steady states  $u(x) \equiv \text{constant}$  available to start the continuation as in Section 3. This makes (30) substantially more difficult.

The homotopy continuation strategy (II) with branch switching from Section 3 is now extremely complicated to carry out. One option is to set  $\gamma_a = 0$ , then start with the zero solution, compute the different non-trivial branches using strategy (II), and then continue each branch also in the parameter  $\gamma_a$  up to  $\gamma_a = 10$ . Albeit certainly possible, it is actually a lot easier in this case to follow the gluing strategy (I) as the code can basically be used almost unaltered, just by adding  $\gamma$  and noticing that the new energy functional, for  $\mu = 0$  (cf. equation (25)), is just given by

$$J(u) = \int_{\Omega} \left[ \frac{1}{2} \|\nabla u(x)\|^2 - \frac{1}{4} u^4(x) + u(x)\gamma(x) \right] dx. \quad (32)$$

The results for the continuation runs are shown in Figures 3-5 with `hmax` = 0.07 and `neig` = 200. The results in Figure 3 show the continuation for the  $MI = 1$  solution. The starting solution at  $\mu = 0$  has a peak slightly shifted towards the upper right corner of the domain in comparison to the solution in Figure 1(a). Continuing forward in  $\mu$  leads to the black curve in Figure 3 along which the solution peak shrinks and moves into the top right corner. On this curve, a fold point at  $\mu = \mu_f \approx 2.92$  occurs, at which the unstable starting solution stabilizes. The bottom curve below the fold is expected to be the global attractor for non-steady-state starting solutions in the range of for all  $\mu \in (-\infty, \mu_f]$  for the associated parabolic PDE.

Running the continuation backwards, i.e. with step size  $-\delta s$ , yields the grey curve. Along this curve, the solution peak increases and also moves into the top right corner. We also continued both parts of the “(reflected) C-shaped” branch up to  $\mu = -100$  and no branching was detected. In fact, the branch shape remains, only the peaks seem to sharpen. In fact, a mesh refinement was helpful for the upper part of the curve as discussed in Section 2.1. The sharpening of the peaks is expected from a formal scaling argument since we can re-write (30) for  $\mu \neq 0$  as

$$\begin{cases} 0 = -\frac{1}{\mu}\Delta u - u - \frac{1}{\mu}u^3 + \frac{1}{\mu}\gamma, & x \in \Omega, \\ 0 = u, & x \in \partial\Omega, \end{cases} \quad (33)$$

which is a singularly perturbed elliptic PDE as  $|\mu| \rightarrow +\infty$  (here  $\mu \rightarrow -\infty$ ). For singularly perturbed elliptic PDEs, concentration phenomena, spike- and/or boundary-layer solutions are a common phenomenon [78, 85, 86]. More detailed numerical performance calculations were also carried out for this branch and are discussed in Appendix A.

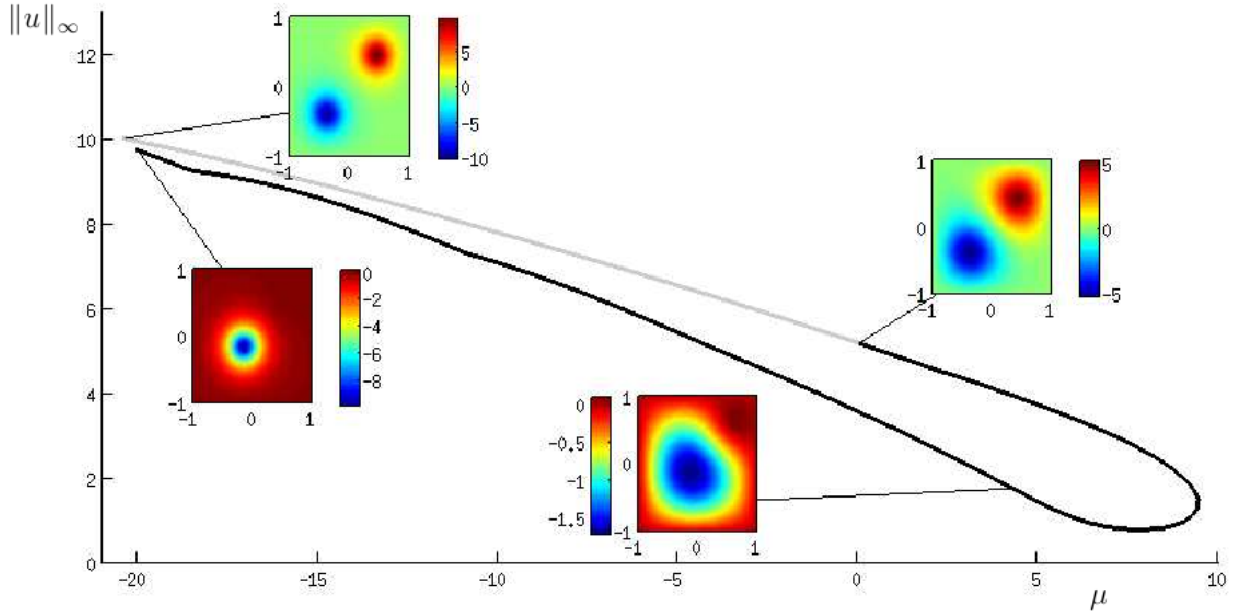


Figure 4: Numerical continuation results for (30) with external force given by (31). The starting solution was obtained by the variational minimax approach at  $\mu = 0$ . Then forward and backward numerical continuation from this starting point leads to two branches (black and grey). The starting solution with Morse index  $MI = 2$  is also shown; for a more detailed description see the main text.

In Figure 4, a starting solution from the minimax approach with  $MI = 2$  and two peaks along the diagonal is considered. Interestingly, along the lower (black) branch of solutions, there is a deformation from a two-peak solution with one minimum and one maximum to a single minimum solution. Along the upper (grey) branch, the two-peak structure remains to hold. Again, we have a C-shaped branch, which folds even tighter back towards itself in the  $L^\infty$ -norm. Continuing back towards  $\mu = -100$  did not lead to the detection of bifurcation

points so we may actually conjecture that the symmetry-breaking leads to various isolas corresponding to different peak-structure solutions.

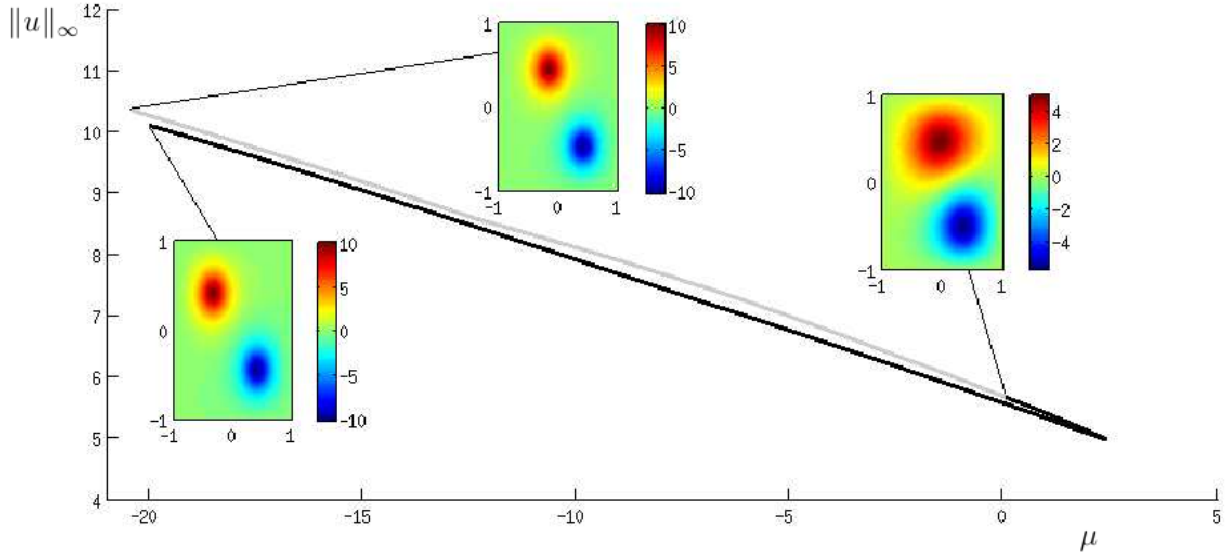


Figure 5: Numerical continuation results for (30) with external force given by (31). The starting solution was obtained by the variational `minimax` approach at  $\mu = 0$ . Then forward and backward numerical continuation from this starting point leads to two branches (black and grey). The starting solution with Morse index  $MI = 2$  is also shown. Note that this starting solutions is different from the one in Figure 4; for a more detailed description see the main text.

We also used the `minimax` method to find another two-peak saddle-solution shown as the starting solution in Figure 5. This starting solutions has  $MI = 2$  and a slightly broader peak near the top left corner in comparison to the peak in the lower right corner. As before, we applied the same forward and backward continuation steps and obtain another C-shaped branch, which does not connect to any other solutions up to  $\mu = -100$  and is likely to be isolated from other branches. However, in comparison to the case of Figure 4, there is no change in the peak structure along the branch and the turning in the  $L^\infty$ -norm is even tighter.

In summary, the `minimax` starting strategy turned out to be computationally simple and quite effective to determine starting solutions. Furthermore, we may conclude for the Lane-Emden-Fowler equation (30) with microforce (31) that symmetry-breaking by external forces can lead to quite interesting bifurcation branch structures, splitting the various branches, which are connected to  $u \equiv 0$  when  $\gamma = 0$  as shown in Section 3. There seem to be many open questions regarding the global bifurcation structure for various forces, even for simple elliptic problems in the plane. Although the global structure is easily accessed numerically, one may hope to understand the problem near a bifurcation point of the trivial branch for  $0 < |\gamma(x)| \ll 1$  analytically by a perturbation argument and local unfolding; again, this questions seems to be open for different microforces.

## 5 The Caginalp System

In addition to the previous two case studies in Sections 3-4, where the `minimax` starting solutions have been used according to approach (I), one may also ask for an example where the classical continuation approach is preferable but gluing computation still plays an important role.

Consider again a compact domain  $\Omega \subset \mathbb{R}^2$ , which represents a material or body, and let  $(x, t) \in \Omega \times [0, T]$ . The Caginalp system models the interaction between a phase field (or order parameter)  $\chi = \chi(x, t)$  and the temperature  $\vartheta = \vartheta(x, t)$ . It was originally proposed in [22] and studied using many different techniques [50, 84]. From the modelling perspective, it describes, e.g., melting-solidification processes between different pure phases. Here we use a version of the Caginalp system in the scaling considered in [51] given by

$$\left\{ \begin{array}{ll} \frac{\partial \vartheta}{\partial t} + \frac{\partial}{\partial t} \lambda(\chi) = \Delta \vartheta + f, & \text{if } (x, t) \in \Omega \times [0, T], \\ \frac{\partial \chi}{\partial t} = \Delta \chi - (DW)(\chi) + (D\lambda)(\chi)\vartheta, & \text{if } (x, t) \in \Omega \times [0, T], \\ 0 = \vartheta, & \text{if } (x, t) \in \partial\Omega \times [0, T], \\ 0 = \vec{n} \cdot \nabla \chi, & \text{if } (x, t) \in \partial\Omega \times [0, T], \\ \vartheta = \vartheta_0, & \text{if } (x, t) \in \Omega \times \{0\}, \\ \chi = \chi_0, & \text{if } (x, t) \in \Omega \times \{0\}, \end{array} \right. \quad (34)$$

where  $W : \mathbb{R} \rightarrow \mathbb{R}$  is a given potential,  $f : \Omega \rightarrow \mathbb{R}$  is a heat source/sink and  $\lambda : \mathbb{R} \rightarrow \mathbb{R}$  models the latent heat density. We are just interested in the stationary Caginalp system under a given fixed heat source. In this case, the system reduces to

$$\left\{ \begin{array}{ll} 0 = \Delta \vartheta + f, & \text{if } x \in \Omega, \\ 0 = \Delta \chi - (DW)(\chi) + (D\lambda)(\chi)\vartheta, & \text{if } x \in \Omega, \\ 0 = \vartheta, & \text{if } x \in \partial\Omega, \\ 0 = \vec{n} \cdot \nabla \chi, & \text{if } x \in \partial\Omega, \end{array} \right. \quad (35)$$

where all unknown functions  $\chi = \chi(x), \vartheta = \vartheta(x)$  only depend upon the spatial variable. Returning to one modelling purpose of the Caginalp system, namely melting-solidification processes, we aim to chose a domain  $\Omega \subset \mathbb{R}^2$  on which melting and solidification definitely play a crucial role in applications. One engineering application of interest are airplane wings, where the process of avoiding ice formation is of critical importance [100]. So we chose  $\Omega$  as a very basic wing-shaped domain as shown in Figure 6.

A first step for the numerical continuation of (35) is to note that we may use an offline pre-computing step since we have assumed that  $f$  is time-independent, i.e., we may solve a Poisson equation

$$\left\{ \begin{array}{ll} 0 = \Delta \vartheta + f, & \text{if } x \in \Omega, \\ 0 = \vartheta, & \text{if } x \in \partial\Omega. \end{array} \right. \quad (36)$$

In this context, a gluing framework is very helpful. It is very easy to use the graphical user-interface provided by the `pdetoolbox` to define the domain  $\Omega$ , specify  $f$ , the Dirichlet boundary conditions, the PDE itself, and then solve the Poisson equation (36). The solution for  $f \equiv 2000$  is shown in Figure 6. Hence, if we view  $\vartheta(x) = \vartheta$  as a known temperature

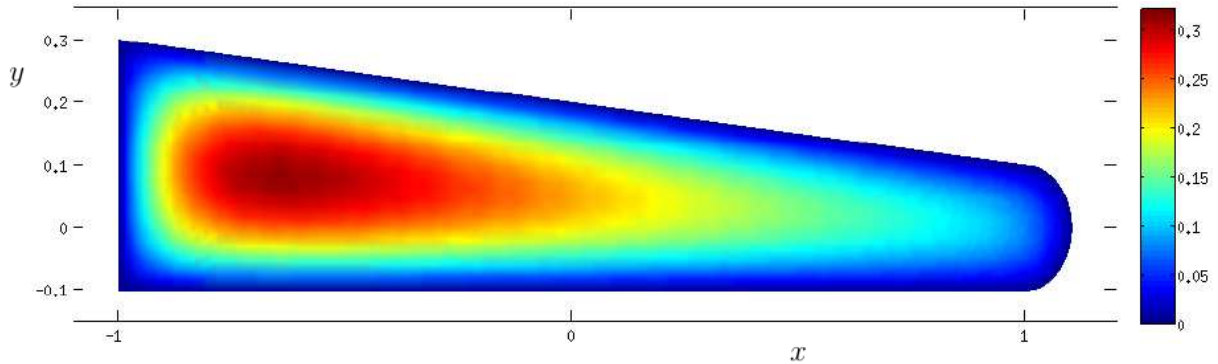


Figure 6: Solution of the Poisson equation (36) computed over the basic wing-shaped domain  $\Omega$  with a constant point heat source  $f \equiv 2 \cdot 10^3$ . This solution is used as an input to the Caginalp system (37).

input for the Caginalp system (35) then it remains to study

$$\begin{cases} 0 = -\Delta\chi + (DW)(\chi) - (D\lambda)(\chi)\vartheta, & \text{if } x \in \Omega, \\ 0 = \vec{n} \cdot \nabla\chi, & \text{if } x \in \partial\Omega, \end{cases} \quad (37)$$

as an elliptic PDE for the order parameter  $\chi$ .

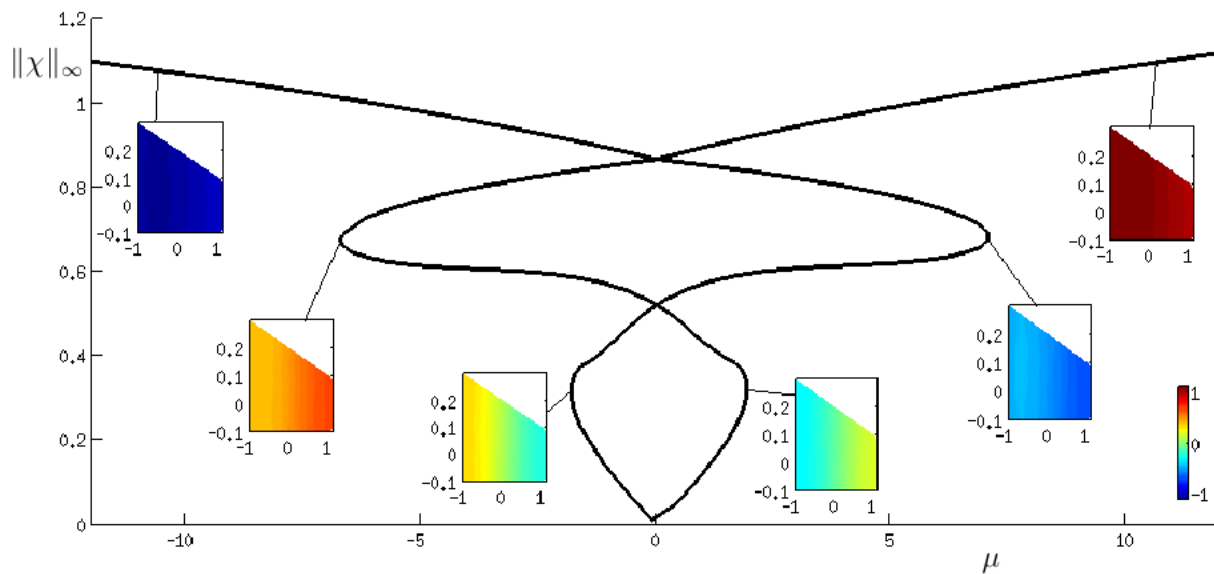


Figure 7: Numerical continuation results for (37) with  $\vartheta = \vartheta(x)$  from Figure 6, latent heat density (38) and potential (39). The starting solution was computed for  $\mu = 1$  by iterating an initial guess. The remaining part of the diagram was computed using continuation in `pde2path`. For a more detailed description see the main text.

To study the reduced Caginalp equation (37) numerically, we still have to specify the form of the latent heat density  $\lambda : \mathbb{R} \rightarrow \mathbb{R}$  and the potential  $W : \mathbb{R} \rightarrow \mathbb{R}$ . The latent heat density

is frequently modeled and/or empirically determined as leading-order affine-linear term with higher-order small-prefactor nonlinear polynomial correction terms [89]. To replicate this modelling, we just consider

$$\lambda(\tau) := \mu (c_0 + c_1\tau + c_2\tau^2), \quad (38)$$

where  $\mu$  is again the bifurcation parameter and  $c_1 = 1$  and  $c_2 = 0.05$  are fixed for the computation; note that  $c_0$  is not relevant here as only  $D\lambda$  appears in (37). For the potential, we select the standard example

$$W(y) := (y^2 - 1)^2, \quad (39)$$

which was already studied by Caginalp [22]. Note carefully, that the elliptic PDE (37) has a variational structure with energy functional

$$J(\chi) = \int_{\Omega} \left[ \frac{1}{2} \|\nabla\chi(x)\|^2 + W(\chi) - \lambda(\chi(x))\vartheta(x) \right] dx. \quad (40)$$

However, the quartic term  $\chi^4$  has a positive sign, i.e., the Allen-Cahn/Ginzburg-Landau sign and not the Lane-Emden-Fowler sign. Still one may formally try to apply a minimax approach but the `minimax` code [108] we used for Sections 3-4 does not yield multiple solutions, even upon minor modifications. Hence, a deeper modification, or a completely different approach would be required to scan for multiple solutions at a fixed parameter value.

Naturally, we first have to make sure there really are multiple solutions for some fixed parameter value. In this case, the continuation approach can be used to find these solutions. In particular, we start at  $\mu = 1$  by guessing a constant solution. Under Newton iteration, we actually do reach a true solution of the problem for  $\mu = 1$ . Then we can use numerical continuation to track the solution branch as shown in Figure 7. We observe that there are at least four different solutions at  $\mu = 1$  so there should definitely be a variational approach to determine them systematically and we leave this problem as an open problem for future numerical work<sup>12</sup>.

The bifurcation diagram in Figure 7 is quite interesting for applications so we briefly comment on the results. We cut off the bifurcation diagram and only consider the region with  $\|\chi\|_{\infty} \leq 1$  as  $\chi = \pm 1$  represent the pure states and we are interested in the transition (or so-called mushy) regime between the pure states. Suppose we start in the bifurcation diagram with an (almost) pure state  $\chi(x) \approx 1$  for all  $x \in \Omega$  and then change  $\mu$ . This leads to a transition sequence involving four folds as shown in Figure 7. If we interpret  $\chi(x) \approx 1$  as a melted (or liquid) state, then the solution curve at the first fold assumes a mixed/mushy state where solidification starts non-uniformly over the domain, with a focus near the airplane body. This focus reverses as the solution branch is traversed further and at the third fold, when the solidification focuses on the tip. In the last step, the system transitions to the almost fully solid state after the fourth fold has been traversed. Although we shall not pursue these ideas here further, it is clear that these observations should have interesting applications in engineering applications to build airplane wings and/or during a de-icing process. We leave a detailed parametric numerical continuation study for melting/solidification processes for future work.

---

<sup>12</sup>It is likely that there is a variational algorithm available to search for multiple solutions in this case but not one, which is freely available for the direct gluing computation approach proposed here.

## 6 Perspectives on Software Development

Although we have successfully demonstrated that gluing computing between FEM, continuation and minimax can be efficient and lead to very interesting practical results for elliptic PDEs, we have not commented on several important practical scientific computing issues. In particular, the question is why the computations here worked in a relatively straightforward way, while gluing computation can become very complicated in many cases when one tries to track patterns via numerical continuation; the thesis [8] is an excellent example, how challenging such a computational approach can become. The following issues seem to be very helpful to keep in mind for further software development<sup>13</sup>:

**High-level language:** A key ingredient to efficiently glue different parts required for the computation is to use a high-level programming language. Here `MatLab` [81] is used. However, an excellent non-commercial alternative would be `Python` [104], which contains aspects designed for gluing computation and is already efficiently used in various scientific computing packages for differential equations [42, 58, 53, 30, 57]. The problem with working directly with FEM, continuation or variational-PDE packages via a fast-computation, but lower-level, programming language, e.g. `C`, `C++` or `Fortran`, is that even apparently simple-looking tasks of transferring data, adding on functionality, problem formulation, interlinking of algorithms, cross-validation, testing and visualization, become incredibly complicated and time-consuming. To really make a gluing approach work on the basis of a lower-level language, one has to fully integrate multiple software packages into a single, necessarily constrained, environment. Although this may be very desirable in standardized industrial applications, it does not adequately represent software development and flexibility requirements in an academic environment. Only a higher-level language provides the required flexibility. Of course, ones has to give up a slight bit of computational efficiency but overall, this trade-off seems worthwhile.

In this context, it should be noted that such an integration of input-output via a high-level language should probably be made a design principle from the start. If wrapper-functionality is added later on, it is frequently still necessary to fully comprehend the underlying low-level code to actually use the wrapper.

**Algorithmic blocks:** Based upon the previous point, one should make sure to design self-consistent blocks of code, which interface/communicate directly with a high-level language but run on a lower-level fast language for computational purposes. For example, in the context considered in this paper one might want to split up the process into the following components:

- (A1) problem formulation and definitions;
- (A2) mesh generation and error-estimator based mesh refinement;
- (A3) discretization of the PDE, i.e., conversion to a nonlinear algebraic system;
- (A4) algorithms for generating starting solutions sets;

---

<sup>13</sup>Of course, the various issues are written from the viewpoint of a user in applied nonlinear dynamics, who is interested in gluing computations.

- (A5) numerical continuation and bifurcation detection;
- (A6) efficient, fast numerical linear algebra;
- (A7) data analysis and visualization.

Of course, not all the different steps are necessary for a given class of PDEs or chosen discretization algorithm. For example, sometimes one may omit (A4) due to the availability of starting solutions as for approach (II) in Section 3, or use spectral or other mesh-free methods to generate the nonlinear system of algebraic equations to be solved in (A3).

**Problem description:** Another natural question is, how we should formulate the PDE meshing, discretization and continuation problem in the high-level gluing language? In this regard, `pde2path` builds upon the successful ideas implemented in `AUTO`. The main idea is to have only very few files that specify all the problem details completely: one (or two) files to specify the elliptic PDE, one file to initialize all the data (domain, initial guess, algorithmic parameters, etc.) and one structure to track the current state of the numerical problem. Those ideas turned out, again, to be extremely robust and helpful to carry out the gluing computations in this paper. We also completely glued the `minimax`-algorithm [108] to `pde2path` by using only data from standard `pde2path` problem description files in `minimax`. In principle, this could be implemented permanently into `pde2path` but there is a new version released soon [43]. The variational starting solution approach will be implemented in this new version in future work<sup>14</sup>.

**PDE discretization:** By now, there are a large number of different software packages available to automatically generate meshes, nonlinear equations and adaptive mesh refinements for various classes of PDEs; see Section 1. Many of these software packages would provide excellent tools for understanding dynamics and patterns in a wide variety of applications a lot better. In fact, the barrier does not lie in the packages themselves but the difficulty to access the problem formulation. For example, it is relatively rare that one can simply provide a problem description and obtain, *in a simple format*, the discretized nonlinear equations as an output; of course, it is always *possible* but the goal is to make gluing computation *easy*. However, there seems significant progress in this direction, e.g. see [58]. The demonstration we have given here for three problems also strongly points towards the conjecture that practical gluing computations for dynamical systems analysis of PDEs will become a lot easier in the very near future.

**Continuation algorithms:** The main barrier to make continuation algorithms more applicable to spatial problems was to move beyond the class of two-point BVPs and provide a more generic package suitable for PDEs. This is one current disadvantage with the `pde2path` focus we considered in this paper since `pde2path` links internally a continuation algorithm directly to the MatLab `pdetoolbox`. Therefore, it is not easy in practice to replace the steps (A3) and (A5) as they are tied together in `pde2path`. However, this could be resolved by using a generic continuation toolbox, such as the recently developed continuation core `COCO` [33] or certain tools for large-dimensional linear systems such as `LOCA` [91] or other recently

---

<sup>14</sup>The new version `p2p2` is not backward compatible with `pde2path` so we postpone this step to future work. It is expected that compatibility is guaranteed from the version `p2p2` onwards [43].

developed codes [19]. The main point is, that in the future one must take advantage of the advanced numerical analysis discretization schemes to reduce the computational linear algebra effort more efficiently. Overall, there is also significant recent progress in this direction supporting the conjecture stated in the last paragraph.

## 7 Summary

In this paper we have addressed the issue of gluing computation at the interface between numerical PDEs, continuation methods, scientific computing and variational theory in the context of elliptic PDEs for three different equations. We have shown that efficient integration of various algorithms within the framework of a high-level programming framework can be possible. A combination of `pde2path`, the MatLab `pdetoolbox` and a `minimax`-algorithm has been glued and cross-validated using the Lane-Emden-Fowler equation with a linear term as a test problem. As a second step, we argued that a natural symmetry-breaking mechanism, which is not based upon the domain geometry, could be localized asymmetric microscopic forces which also arise in generalized Ginzburg-Landau/Allen-Cahn equations. We found interesting inverse-C-shaped bifurcation curves. There is numerical evidence to conjecture that these curves are isolas, which could be analytically captured in the regime of a very small microforce. Along the bifurcation curves, complicated deformation of patterns can already take place under a simple near-localized external microforce. Then we proposed to study as a third example the Caginalp system for melting-solidification processes on a wing-shaped geometry. In this case, the variational `minimax`-algorithm could not directly be glued despite the existence of multiple solutions at fixed parameters. This illustrated the limitations of the process. For the Caginalp system, we also computed an interesting phase transition diagram for melting-solidification processes, which pointed towards potentially useful aerospace and engineering applications. Finally, we also commented on scientific computing issues encountered during the process.

**Acknowledgments:** I would like to thank the Austrian Academy of Sciences (ÖAW) for support via an APART fellowship. I also acknowledge support of the European Commission (EC/REA) via a Marie-Curie International Re-integration Grant. I would like to thank John Guckenheimer, Hannes Uecker and Mathieu Desroches for very helpful comments on earlier versions of this manuscript. Furthermore, I would like to thank two anonymous referees, whose comments have helped to improve the paper.

## 8 References

### References

- [1] S.M. Allen and J.W. Cahn. A microscopic theory for antiphase boundary motion and its application to antiphase domain coarsening. *Acta Metallurgica*, 27(6):1085–1905, 1979.
- [2] E.L. Allgower and K. Georg. *Introduction to Numerical Continuation Methods*. SIAM, 2003.
- [3] W. Ao, J. Wei, and J. Zeng. An optimal bound on the number of interior spike solutions for the lin-ni-takagi problem. *J. Funct. Anal.*, 265(7):1324–1356, 2013.

- [4] I.S. Aranson and L. Kramer. The world of the complex Ginzburg-Landau equation. *Rev. Mod. Phys.*, 74:99–143, 2002.
- [5] D.N. Arnold, F. Brezzi, B. Cockburn, and L.D. Marini. Unified analysis of discontinuous Galerkin methods for elliptic problems. *SIAM J. Numer. Anal.*, 39(5):1749–1779, 2002.
- [6] U. Ascher, J. Christiansen, and R.D. Russell. COLSYS-A collocation code for boundary-value problems. In *Codes for Boundary-Value Problems in Ordinary Differential Equations*, pages 164–185. Springer, 1979.
- [7] U.M. Ascher, R.M.M. Mattheij, and R.D. Russell. *Numerical Solution of Boundary Value Problems for Ordinary Differential Equations*. SIAM, 1987.
- [8] D. Avitabile. *Computation of planar patterns and their stability*. PhD thesis, University of Surrey, 2008.
- [9] D. Avitabile, M. Desroches, and S. Rodrigues. On numerical continuation of isolas of equilibria. *Int. J. Bif. Chaos*, 22(11):1250277, 2012.
- [10] D. Avitabile, D.J.B. Lloyd, J. Burke, E. Knobloch, and B. Sandstede. To snake or not to snake in the planar Swift-Hohenberg equation. *SIAM J. Appl. Dyn. Syst.*, 9(3):704–733, 2010.
- [11] P.K. Banerjee and R. Butterfield. *Boundary Element Methods in Engineering Science*. McGraw-Hill, 1981.
- [12] W. Bangerth and T. Heister. Quo vadis, scientific software? *SIAM News*, 47(1):8, 2014.
- [13] D. Barkley. Linear stability analysis of rotating spiral waves in excitable media. *Phys. Rev. Lett.*, 68(13):2090–2093, 1992.
- [14] D. Barkley, I.G. Kevrekidis, and A.M. Stuart. The moment map: nonlinear dynamics and density evolution via a few moments. *SIAM J. Appl. Dyn. Syst.*, 5(3):403–434, 2006.
- [15] T. Bartsch, T. D’Aprile, and A. Pistoia. Multi-bubble nodal solutions for slightly subcritical elliptic problems in domains with symmetries. *Ann. Inst. Henri Poincaré (C)*, 30(6):1027–1047, 2013.
- [16] M. Beck, J. Knobloch, D.J. Lloyd, B. Sandstede, and T. Wagenknecht. Snakes, ladders, and isolas of localized patterns. *SIAM J. Math. Anal.*, 41(3):936–972, 2009.
- [17] P. Beltrame and U. Thiele. Time integration and steady-state continuation method for lubrication equations. *SIAM J. Appl. Dyn. Syst.*, 9:484–518, 2010.
- [18] W.-J. Beyn. The numerical computation of connecting orbits in dynamical systems. *IMA J. Numer. Anal.*, 9:379–405, 1990.
- [19] D. Bindel, M. Friedman, W. Govaerts, J. Hughes, and Yu.A. Kuznetsov. Numerical computation of bifurcations in large equilibrium systems in MATLAB. *J. Comp. Appl. Math.*, 261:232–248, 2014.
- [20] S.C. Brenner and L.R. Scott. *The Mathematical Theory of Finite Element Methods*. Springer, 3rd edition, 2008.
- [21] R.E. Caflisch. Monte Carlo and quasi-Monte Carlo methods. *Acta Numerica*, 7:1–49, 1998.
- [22] G. Caginalp. An analysis of a phase field model of a free boundary. *Arch. Rat. Mech. Anal.*, 92:205–245, 1986.

- [23] G. Caginalp and P.C. Fife. Dynamics of layered interfaces arising from phase boundaries. *SIAM J. Appl. Math.*, 48(3):506–518, 1988.
- [24] A.R. Champneys, Yu.A. Kuznetsov, and B. Sandstede. A numerical toolbox for homoclinic bifurcation analysis. *Int. J. of Bif. and Chaos*, 6(5):867–887, 1996.
- [25] S. Chandrasekhar. *An Introduction to the Study of Stellar Structure*. Dover, 2010.
- [26] G. Chen, J. Zhou, and W.-M. Ni. Algorithms and visualization for solutions of nonlinear elliptic equations. *Int. J. Bifur. Chaos*, 10(7):1565–1612, 2000.
- [27] X. Chen and J. Zhou. On homotopy continuation method for computing multiple critical points. *Numer. Meth. Partial Differential Equat.*, 24(3):728–748, 2008.
- [28] X. Chen and J. Zhou. A local min-max-orthogonal method for finding multiple solutions to noncooperative elliptic systems. *Math. Comput.*, 79:2213–2236, 2010.
- [29] Y.S. Choi and P.J. McKenna. A mountain pass method for the numerical solution of semi-linear elliptic problems. *Nonl. Anal.: Theor. Meth. Appl.*, 20:417–437, 1993.
- [30] R. Cimrman. SfePy - write your own FE application. In P. de Buyl and N. Varoquaux, editors, *Proceedings of the 6th European Conference on Python in Science (EuroSciPy 2013)*, pages 65–70, 2014. see also <http://arxiv.org/abs/1404.6391>.
- [31] R.H. Clewley, W.E. Sherwood, M.D. LaMar, and J. Guckenheimer. PyDSTool: a software environment for dynamical systems modeling. <http://pydstool.sourceforge.net>, 2010.
- [32] J.A. Cottrell, T.J. Hughes, and Y. Bazilevs. *Isogeometric analysis: toward integration of CAD and FEA*. Wiley, 2009.
- [33] H. Dankowicz and F. Schilder. *Recipes for Continuation*. SIAM, 2013.
- [34] M. Desroches, B. Krauskopf, and H.M. Osinga. The geometry of mixed-mode oscillations in the Olsen model for the peroxidase-oxidase reaction. *DCDS-S*, 2(4):807–827, 2009.
- [35] M. Desroches, B. Krauskopf, and H.M. Osinga. Numerical continuation of canard orbits in slow-fast dynamical systems. *Nonlinearity*, 23(3):739–765, 2010.
- [36] A. Dhooge, W. Govaerts, and Yu.A. Kuznetsov. MATCONT: A MATLAB package for numerical bifurcation analysis of ODEs. *ACM Trans. Math. Softw.*, 29:141–164, 2003.
- [37] H.A. Dijkstra, F.W. Wubs, A.K. Cliffe, E. Doedel, I.F. Dragomirescu, B. Eckhardt, A.Yu. Gelfgat, A.L. Hazel, V. Lucarini, A.G. Salinger, E.T. Phipps, J. Sanchez-Umbria, H. Schuttelaars, L.S. Tuckerman, and U. Thiele. Numerical bifurcation methods and their application to fluid dynamics: analysis beyond simulation. *Commun. Comput. Phys.*, 15(1):1–45, 2014.
- [38] Z. Ding, D. Costa, and G. Chen. A high linking method for sign changing solutions for semilinear elliptic equations. *Nonl. Anal.: Theor. Meth. Appl.*, 38:151–172, 1999.
- [39] E. Doedel, H.B. Keller, and J.-P. Kernevez. Numerical analysis and control of bifurcation problems. I. Bifurcation in finite dimensions. *Internat. J. Bifur. Chaos Appl. Sci. Engrg.*, 1(3):493–520, 1991.
- [40] E. Doedel, H.B. Keller, and J.-P. Kernevez. Numerical analysis and control of bifurcation problems. II. Bifurcation in infinite dimensions. *Internat. J. Bifur. Chaos Appl. Sci. Engrg.*, 1(4):745–772, 1991.

- [41] E.J. Doedel. AUTO, a program for the automatic bifurcation analysis of autonomous systems. *Cong. Numer.*, 30:265–384, 1981.
- [42] E.J. Doedel, A. Champneys, F. Dercole, T. Fairgrieve, Y. Kuznetsov, B. Oldeman, R. Paffenroth, B. Sandstede, X. Wang, and C. Zhang. Auto 2007p: Continuation and bifurcation software for ordinary differential equations (with homcont). <http://cmvl.cs.concordia.ca/auto>, 2007.
- [43] T. Dohnal, J.D.M. Rademacher, H. Uecker, and D. Wetzel. pde2pathv2: multi-parameter continuation and periodic domains. In *ENOC 2014, Vienna*, pages 1–6, 2014.
- [44] K. Engelborghs, T. Luzyanina, and G. Samaey. *DDE-BIFTOOL v. 2.00: a Matlab package for bifurcation analysis of delay differential equations*. KU Leuven, 2000.
- [45] B. Ermentrout. *XPPAUT*. <http://www.math.pitt.edu/~bard/xpp/xpp.html>, 2008.
- [46] L.C. Evans. *Partial Differential Equations*. AMS, 2002.
- [47] D. Gilbarg and N.S. Trudinger. *Elliptic Partial Differential Equations of Second Order*. Springer, 2001.
- [48] D. Gottlieb and S.A. Orszag. *Numerical Analysis of Spectral Methods*. SIAM, 1977.
- [49] W.F. Govaerts. *Numerical Methods for Bifurcations of Dynamical Equilibria*. SIAM, Philadelphia, PA, 1987.
- [50] M. Grasselli, A. Miranville, and G. Schimperna. The Caginalp phase-field system with coupled dynamic boundary conditions and singular potentials. *Discrete Contin. Dyn. Syst. A*, 28(1):67–98, 2010.
- [51] M. Grasselli, H. Petzeltová, and G. Schimperna. Long time behaviour of solutions to the Caginalp system with a singular potential. *Z. Anal. Anwendungen*, 25:51–72, 2006.
- [52] M.E. Gurtin. Generalized Ginzburg-Landau and Cahn-Hilliard equations based on a microforce balance. *Physica D*, 92:178–192, 1996.
- [53] J.E. Guyer, D. Wheeler, and J.A. Warren. FiPy: Partial differential equations with python. *Computing in Science and Engineering*, 11(3):6–15, 2009.
- [54] D. Ter Haar, editor. *Collected Papers of L.D. Landau*. Pergamon Press, 1965.
- [55] S. Heinrich. Multilevel Monte Carlo methods. In *Large-scale Scientific Computing*, pages 58–67. Springer, 2001.
- [56] M.E. Henderson. Multiple parameter continuation: Computing implicitly defined k-manifolds. *Int. J. Bif. Chaos*, 12(3):451–476, 2002.
- [57] M.A. Heroux, A.G. Salinger, R.A. Bartlett, H.K. Thornquist, V.E. Howle, R.S. Tuminaro, R.J. Hoekstra, J.M. Willenbring, J.J. Hu, A. Williams, T.G. Kolda, R.B. Lehoucq, K.R. Long, R.P. Pawlowski, E.T. Phipps, and K.S. Stanley. An overview of the Trilinos project. *ACM Trans. Math. Software*, 31(3):397–423, 2005.
- [58] J. Hoffman, C. Johnson, R.C. Kirby, M.G. Larson, A. Logg, and L.R. Scott. The FEniCS project, 2003.
- [59] C. Johnson and K. Eriksson. Adaptive finite element methods for parabolic problems I: a linear model problem. *SIAM J. Numer. Anal.*, 28:43–77, 1991.
- [60] J. Jost. *Riemannian Geometry and Geometric Analysis*. Springer, 2005.

- [61] C. A. Katsman, H.A. Dijkstra, and M.J. Schmeits. Applications of continuation methods in physical oceanography. *Notes on Numerical Fluid Dynamics*, 74:179–198, 2000.
- [62] H. Keller. Numerical solution of bifurcation and nonlinear eigenvalue problems. In P. Rabinowitz, editor, *Applications of Bifurcation Theory*, pages 359–384. Academic Press, 1977.
- [63] H. Keller. Global homotopies and Newton methods. In C. De Boor and G.H. Golub, editors, *Recent Advances in Numerical Analysis*, pages 73–94. Academic Press, 1979.
- [64] H. Keller. Isolas and perturbed bifurcation theory. In R.L. Sternberg, A.J. Kalinowski, and J.S. Papadakis, editors, *Engineering and Applied Science*, pages 45–52. Marcel Dekker, 1980.
- [65] H. Keller. The bordering algorithm and path following near singular points of higher nullity. *SIAM J. Sci. Comput.*, 4(4):573–582, 1983.
- [66] M. Knees, L.S. Tuckerman, and D. Barkley. Symmetry-breaking bifurcations in one-dimensional excitable media. *Phys. Rev. A*, 46(8):5054–5062, 1992.
- [67] J. Knobloch, D.J. Lloyd, B. Sandstede, and T. Wagenknecht. Isolas of 2-pulse solutions in homoclinic snaking scenarios. *J. Dyn. Diff. Equat.*, 23(1):93–114, 2011.
- [68] B. Krauskopf and H.M. Osinga. Computing geodesic level sets on global (un)stable manifolds of vector fields. *SIAM J. Appl. Dyn. Syst.*, 4(2):546–569, 2003.
- [69] B. Krauskopf, H.M. Osinga, E.J. Doedel, M.E. Henderson, J. Guckenheimer, A. Vladimirov, M. Dellnitz, and O. Junge. A survey of methods for computing (un)stable manifolds of vector fields. *Int. J. Bifurcation and Chaos*, 15(3):763–791, 2005.
- [70] B. Krauskopf, H.M. Osinga, and J. Galán-Vique, editors. *Numerical Continuation Methods for Dynamical Systems: Path following and boundary value problems*. Springer, 2007.
- [71] C. Kuehn. From first Lyapunov coefficients to maximal canards. *Int. J. Bif. and Chaos*, 20(5):1467–1475, 2010.
- [72] C. Kuehn. Deterministic continuation of stochastic metastable equilibria via Lyapunov equations and ellipsoids. *SIAM J. Sci. Comp.*, 34(3):A1635–A1658, 2012.
- [73] T. Küpper, R. Seydel, and H. Troger, editors. *Bifurcation: Analysis, Algorithms, Applications*. Birkhäuser, 1987.
- [74] Yu.A. Kuznetsov. *Elements of Applied Bifurcation Theory*. Springer, New York, NY, 3rd edition, 2004.
- [75] R.J. LeVeque. *Finite Volume Methods for Hyperbolic Problems*. CUP, 2002.
- [76] Y. Li and J. Zhou. A minimax method for finding multiple critical points and its applications to semilinear elliptic PDEs. *SIAM J. Sci. Comp.*, 23:840–865, 2001.
- [77] Y. Li and J. Zhou. Convergence results of a local minimax method for finding multiple critical points. *SIAM J. Sci. Comp.*, 24:865–885, 2002.
- [78] C.S. Lin, W.M. Ni, and I. Takagi. Large amplitude stationary solutions to a chemotaxis system. *J. Differential Equat.*, 72(1):1–27, 1988.
- [79] C.S. Lin, W.M. Ni, and J.C. Wei. On the number of interior peak solutions for a singularly perturbed Neumann problem. *Comm. Pure Appl. Math.*, 60:252–281, 2007.
- [80] D.J.B. Lloyd, B. Sandstede, D. Avitabile, and A.R. Champneys. Localized hexagon patterns of the planar SwiftHohenberg equation. *SIAM J. Appl. Dyn. Syst.*, 7(3):1049–1100, 2008.

- [81] The MathWorks. Matlab 2013b, 2013.
- [82] The MathWorks. PDE Toolbox for MatLab, 2013.
- [83] S. McCalla and B. Sandstede. Snaking of radial solutions of the multi-dimensional Swift-Hohenberg equation: A numerical study. *Physica D*, 239:1581–1592, 2010.
- [84] A. Miranville and R. Quintanilla. Some generalizations of the Caginalp phase-field system. *Applicable Analysis*, 88(6):877–894, 2009.
- [85] W.-M. Ni. Diffusion, cross-diffusion and their spike-layer steady states. *Notices Amer. Math. Soc.*, 45(1):9–18, 1998.
- [86] W.-M. Ni. Qualitative properties of solutions to elliptic problems. In *Stationary Partial Differential Equations*, volume 1 of *Handbook of Differential Equations*, pages 157–233. North-Holland, 2004.
- [87] C.S. Peskin. The immersed boundary method. *Acta Numerica*, 11:479–517, 2002.
- [88] J.D.M. Rademacher and B. Sandstede amd A. Scheel. Computing absolute and essential spectra using continuation. *Physica D*, 229:166–183, 2007.
- [89] R.R. Rogers and M.K. Yau. *A Short Course in Cloud Physics*. Pergamon Press, 1989.
- [90] D. Roose, B. De Dier, and A. Spence, editors. *Continuation and Bifurcations: Numerical Techniques and Applications*. Kluwer, 1990.
- [91] A.G. Salinger, E.A. Burroughs, R.P. Pawlowski, E.T. Phipps, and L.A. Romero. Bifurcation tracking algorithms and software for large scale applications. *Internat. J. Bifur. Chaos Appl. Sci. Engrg.*, 15(3):1015–1032, 2005.
- [92] B. Sandstede and D. Lloyd. Using auto for stability problems. Notes for a mini-course given at the University of Washington in Seattle/Washington see: <http://www.dam.brown.edu/people/sandsted/auto/auto-tutorial.pdf>, 2011.
- [93] F. Schilder, H.M. Osinga, and W. Vogt. Continuation of quasi-periodic invariant tori. *SIAM J. Appl. Dyn. Syst.*, 4(3):459–488, 2005.
- [94] N. Schlömer, D. Avitabile, and W. Vanroose. Numerical bifurcation study of superconducting patterns on a square. *SIAM J. Appl. Dyn. Sys.*, 11(1):447–477, 2012.
- [95] J. Serrin and H. Zou. Non-existence of positive solutions of Lane-Emden systems. *Differen. Integral Equat.*, 9(4):635–653, 1996.
- [96] R. Seydel. *Practical Bifurcation and Stability Analysis*. Springer, 1994.
- [97] R. Szalai, G. Stépán, and S.J. Hogan. Continuation of bifurcations in periodic delay-differential equations using characteristic matrices. *SIAM J. Sci. Comput.*, 28(4):1301–1317, 2006.
- [98] C. Taylor and J.H. Dawes. Snaking and isolas of localised states in bistable discrete lattices. *Phys. Lett. A*, 375(1):14–22, 2010.
- [99] J.W. Thomas. *Numerical Partial Differential Equations: Finite Difference Methods*. Springer, 1995.
- [100] S.K. Thomas, R.P. Cassoni, and C.D. MacArthur. Aircraft anti-icing and de-icing techniques and modeling. *J. Aircraft*, 33(5):841–854, 1996.

- [101] L.S. Tuckerman and D. Barkley. Bifurcation analysis for timesteppers. In E. Doedel and L.S. Tuckerman, editors, *Numerical Methods for Bifurcation Problems and Large-Scale Dynamical Systems*, pages 543–566. Springer, 2000.
- [102] H. Uecker and D. Wetzal. Numerical results for snaking of patterns over patterns in some 2D Selkov–Schnakenberg reaction-diffusion systems. *SIAM J. Appl. Dyn. Syst.*, 13(1):94–128, 2014.
- [103] H. Uecker, D. Wetzal, and J.D.M. Rademacher. pde2path - A Matlab package for continuation and bifurcation in 2D elliptic systems. *Num. Math.: Th. Meth. Appl.*, 7:58–106, 2014.
- [104] G. van Rossum. Python tutorial. Technical Report CS-R9526, Centrum voor Wiskunde en Informatica (CWI), 1995.
- [105] Z.Q. Wang and J. Zhou. A local minimax-Newton method for finding multiple saddle points with symmetries. *SIAM J. Numer. Anal.*, 42(4):1745–1759, 2004.
- [106] J.S. Wong. On the generalized Emden-Fowler equation. *SIAM Rev.*, 17(2):339–360, 1975.
- [107] Z. Xie, Y. Yuan, and J. Zhou. On finding multiple solutions to a singularly perturbed Neumann problem. *SIAM J. Sci. Comput.*, 34(1):A395–A420, 2012.
- [108] J. Zhou. A minimax-Newton method for solving semilinear elliptic PDE for multiple solutions, 2009. <http://www.math.tamu.edu/~j.zhou/minimax.tar>; code downloaded 05/2014.

## A Numerical Performance Tests

In this appendix, we collect some performance data for the numerical continuation calculations. There are two main reasons, why it seems useful to collect those results here: (R1) There is to be relatively little detailed data available for `pde2path` used in combination with the MatLab `pde toolbox` and (R2) we want to verify that the computational speed is sufficient to allow for direct numerical experiments on a current standard desktop computer without long waiting times to access the structure of different bifurcation branches.

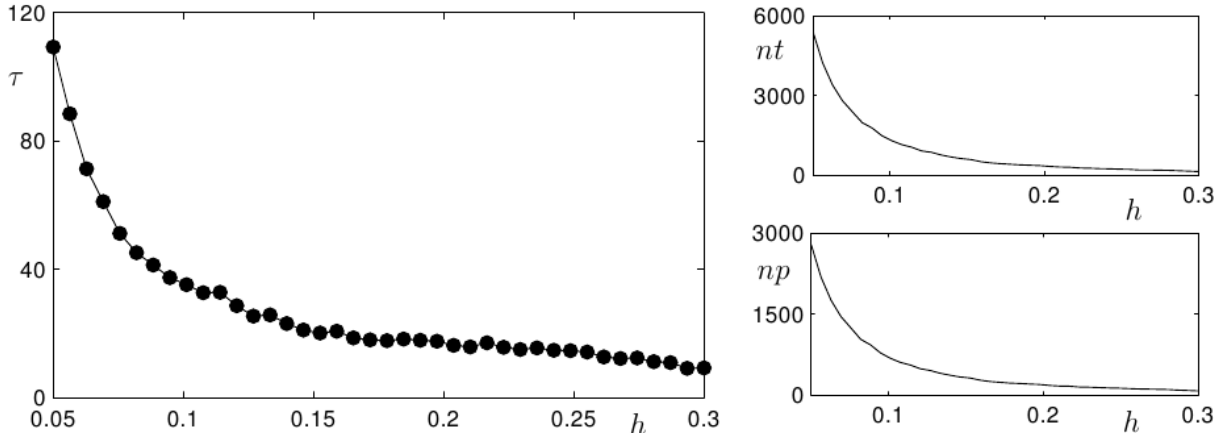


Figure 8: Performance results for continuation calculation of the entire curve in Figure 3 using different meshes with maximal triangle length  $h$ . The panel on the left shows the computing time  $\tau$  in seconds, while the two panels on the right just record the number of points  $np$  and number of triangles  $nt$  in the mesh depending upon  $h$ . The dots mark the computed points in the left figure and the lines are just linear interpolation. In the right part of the figure, the points have been omitted and just the linear interpolation is shown.

As a test problem, we re-compute the branch shown in Figure 3 arising from the Lane-Emden-Fowler equation with a linear term (30) and the external microforce (31). The main reason, why the curve in Figure 3 seems to be a good standard test problem, is that it has a fold point, where the solution changes stability, a single localized solution structure with Morse index one, a singularly-perturbed spike-type structure on the upper branch and a regular smooth solution structure on the lower branch. Hence, despite the algebraic simplicity of the problem, it is expected that many other solution structures for elliptic problems are going to have similar features on bifurcation branches, just with higher Morse indices.

As a first test, we are interested in the influence of mesh size on speed and accuracy of computing the entire branch in Figure 3 using `pde2path`. We use the standard `pde2path` algorithm parameters [103] and only make the following changes

$$\text{p.ds}=0.1, \quad \text{p.tol}=1\text{e-}6, \quad \text{p.xi}=1/\text{p.np}, \quad (41)$$

where `p` is the main dictionary-type continuation structure of `pde2path` and `p.np` is the number of points in the mesh, `p.xi` is the continuation tuning parameter  $\xi$  discussed in Section

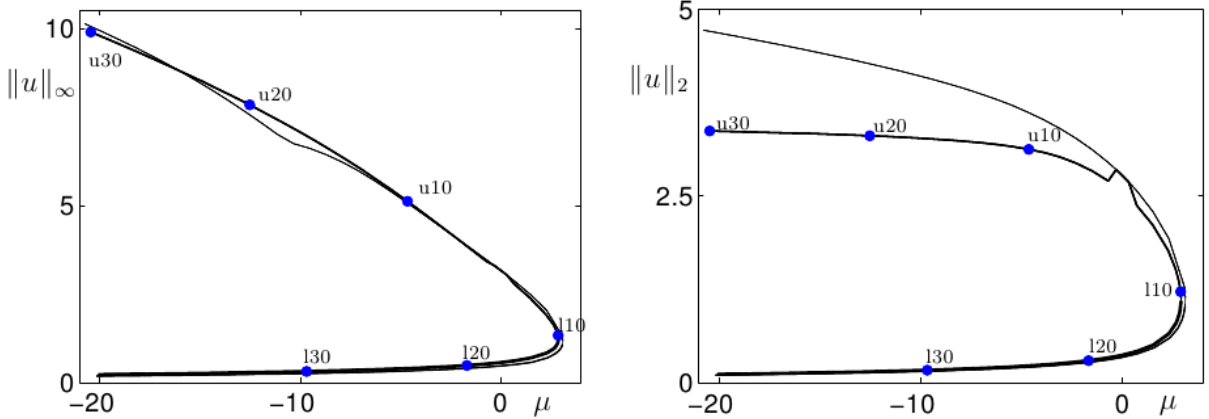


Figure 9: Continuation of the entire curve from Figure 3 using a fixed mesh with  $h = 0.3$  in comparison to an adaptive mesh with parameter (42). The more accurate branch with adaptive meshing has also six different computed points marked on it (in blue), with associated adaptive meshes as shown in Figure 10. Note that in the two figures (left/right) on the norm of the solution is different on the vertical axis i.e., once we use the  $L^\infty(\Omega)$ -norm and once the  $L^2(\Omega)$ -norm.

2.2, `p.tol` is the Newton solver tolerance and `p.ds` the initial continuation step size. We use a maximum triangle edge length of  $h$  and initialize the mesh via `stamemesh` of `pde2path` respectively `initmesh` of the `pdetoolbox`, which yields a Delaunay triangulation of the domain. We run the entire continuation, with spatial mesh adaptation turned off (`p.amod=0`) of the curve shown in Figure 3 for different values of  $h$ . The computation time results are shown in Figure 8. For a quite wide range of mesh sizes the calculation is sufficiently fast to obtain the entire bifurcation curve on a standard current desktop computer<sup>15</sup>.

Then, it is natural to ask about the accuracy of the calculation and which dynamical features are captured along the continuation branch in comparison to the mesh size. In Figure 9 we show the bifurcation curve computed once with a fixed maximum mesh triangle size mesh  $h = 0.3$  in comparison to the case with mesh adaptation as discussed in Section 2.1. The mesh adaptation was chosen by setting

$$\text{p.amod}=5, \quad \text{p.ngen}=10, \quad \text{p.maxt}=4000, \quad (42)$$

in `pde2path`, which means that mesh adaptation is performed every 5 steps along the bifurcation branch and one aims for a maximum number of 4000 triangles in at most 10 refinement steps as discussed in Section 2.1. Note that the solution branch in the  $L^\infty(\Omega)$ -norm is very well-captured, even on the coarse mesh without mesh adaptation. However, on the upper part of the bifurcation branch, decreasing  $\mu$  leads to a singularly-perturbed problem as discussed in Section 4 and the  $L^2(\Omega)$ -norm of the two computations clearly differs. The kink on the branch in the  $L^2(\Omega)$ -norm for the lower curve arises from the fact that the continuation

<sup>15</sup>Basic details of the desktop computer setup used: Intel Core i5-4430 CPU @ 3.00GHz processor (quad-core), Kingston 16GB system memory, WDC WD10EZR00L 1TB harddrive, Ubuntu 12.04.4 LTS operating system, MatLab R2013a computational platform.

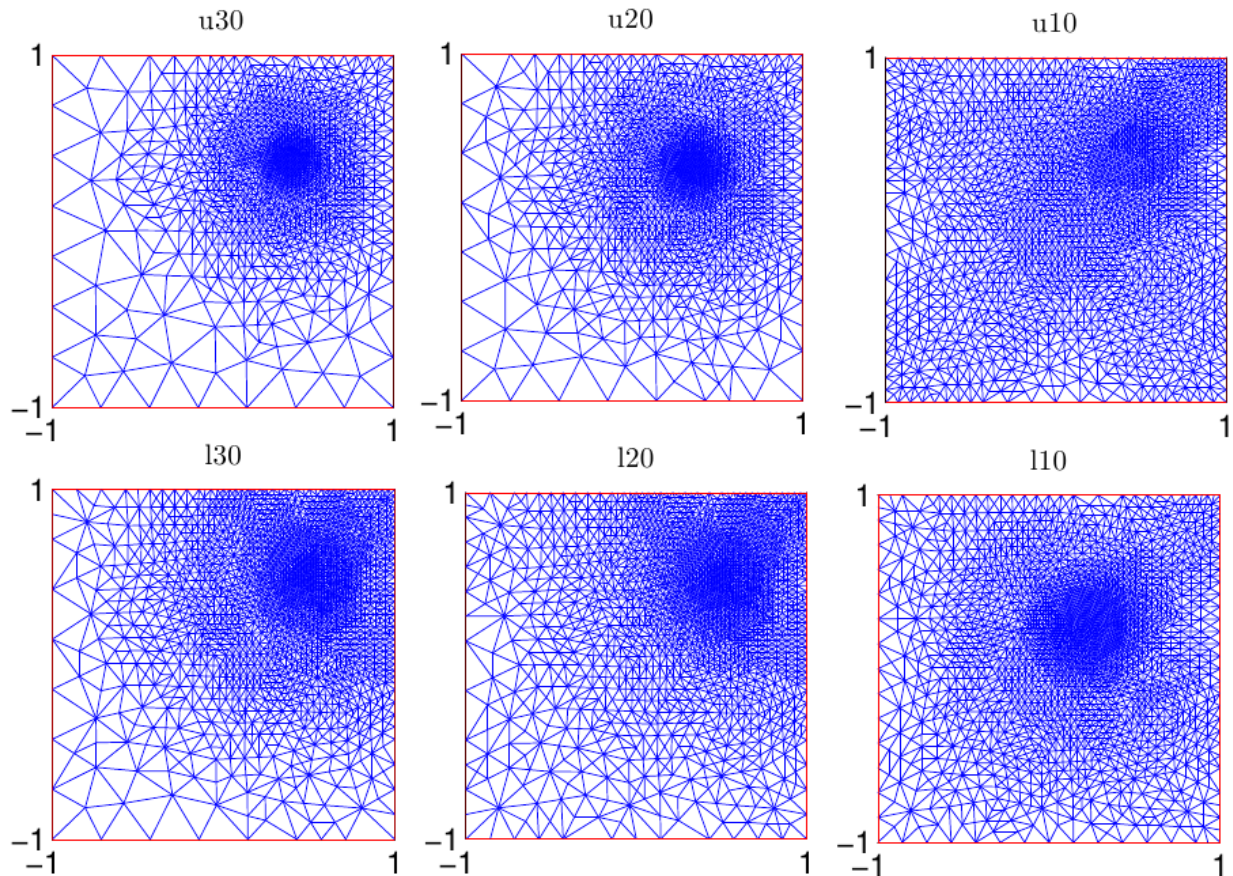


Figure 10: Different adaptive meshes corresponding to the points marked in blue in Figure 9. Observe that the effect of trying to automatically focus on the spike solution for the singularly-perturbed case along the upper branch is clearly visible in the solutions  $u_{20}$  and  $u_{30}$ . On the lower branch, the solution is still localized but does not develop a sharp large spike.

is started with a coarse mesh ( $h = 0.3$ ) and then mesh adaptation only starts to act at the fifth point and corrects the solution norm to its actual value.

Figure 10 demonstrates that the mesh is automatically adapted exactly around the forming spike solution as  $\mu$  decreases. Therefore, we could also have found the singularly-perturbed nature of the problem without the scaling argument leading to equation (33) in an efficient and immediate way. Note that the branches in Figure 9 are expected to diverge in the  $L^2(\Omega)$ -norm as the coarse mesh solution (upper branch) cannot resolve this norm near a spike correctly. However, all indications point to the fact that this is the same branch as the maximum, the region where the solution is nonzero as well as the shape of the spike are the same. It has also been checked that the Newton solver tolerance does not seem to affect the continuation run as the same branch was obtained for all  $\text{p.tol} \in (10^{-11}, 10^{-3})$ .

In Figure 11(a), we investigate the dependence of the continuation time upon the algorithmic tuning parameter  $\xi$  as discussed in Section 2.2. The vertical dashed line marks the suggested setting taking  $\xi$  as the inverse number of points in the mesh  $\text{p.xi}=1/\text{p.np}$ . Inter-

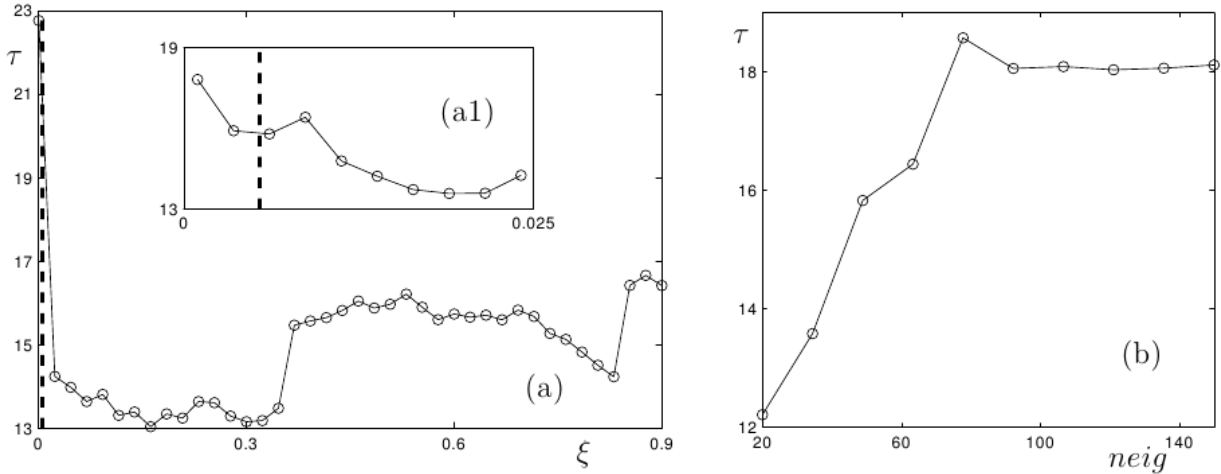


Figure 11: Dependence of the continuation calculations on the parameter  $\xi$  (see Section 2.2) and the number of eigenvalues calculated. Again the entire curve from Figure 3 is calculated for different sets of algorithmic parameters. The circles mark the computed points and the lines are just linear interpolation again. (a) Shows a variation of  $\xi$  plotted against the computing time  $\tau$  (in seconds). The vertical dashed thick line is the suggested value of  $\xi$  from [103]. The inset (a1) shows a finer computation near this suggested value. (b) Computation time depending on the number of eigenvalues  $neig$  computed to determine stability.

estingly, this setting does not seem to be the best from the computational efficiency point of view as it becomes more difficult to track the branch around the fold point. However, choosing  $\xi$  large is also not good as this makes the more horizontal parts of the branch slower to track.

In Figure 11(b), the role of the computation time depending upon the number of eigenvalues calculated  $p.neig$  is considered. Obviously, we expect that the computational effort increases, when more eigenvalues are requested. However, there seems to be at least some saturation effect. Hence, we may conclude that there is certainly potential to optimize continuation runs via algorithmic parameters in the case that larger systems, or many solution branches, are to be considered.